

Noble Dark Matter: Surprising Elusiveness of Dark Baryons

Pouya Asadi,^{1,*} Austin Batz,^{1,†} and Graham D. Kribs^{1,‡}

¹*Institute for Fundamental Science and Department of Physics,
University of Oregon, Eugene, OR, 97403, USA.*

Dark matter could be a baryonic composite of strongly-coupled constituents transforming under $SU(2)_L$. We classify the $SU(2)_L$ representations of baryons in a class of simple confining dark sectors and find that the lightest state can be a pure singlet or a singlet that mixes with other neutral components of $SU(2)_L$ representations, which strongly suppresses the dark matter candidate's interactions with the Standard Model. We focus on models with a confining $SU(N_c)$ and heavy dark quarks constituting vector-like N_f -plet of $SU(2)_L$. For benchmark N_c and N_f , we calculate baryon mass spectra, incorporating electroweak gauge boson exchange in the non-relativistic quark model, and demonstrate that above TeV mass scales, dark matter is dominantly a singlet state. The combination of this singlet nature with the recently discovered \mathcal{H} -parity results in an inert state analogous to noble gases, hence we coin the term Noble Dark Matter. Our results can be understood in the non-relativistic effective theory that treats the dark baryons as elementary states, where we find singlets accompanying triplets, 5-plets, or more exotic representations. This generalization of WIMP-like theories is more difficult to find or rule out than dark matter models that include only a single $SU(2)_L$ multiplet (such as a Wino), motivating new searches in colliders and a re-analysis of direct and indirect detection prospects in astrophysical observations.

Table of Contents

I. Introduction	1	4. Scalar Quarks	19
II. The Theory	2	C. Further Details on the Mass Calculation	21
A. \mathcal{H} -parity from the Ultraviolet	2	1. The Mass Hamiltonian	21
B. Baryon Representations in the Infrared	3	2. Quark Mass Splittings	22
III. Masses in the Heavy Quark Limit	4	3. Spin-flavor Matrix Elements	23
A. Electroweak Contributions in the Quark Model	4	4. Spatial Expectation Values	25
B. Mass Spectra from the Variational Method	4	References	29
IV. Phenomenology	5		
A. Direct Detection	5	I. INTRODUCTION	
B. Indirect Detection and Astrophysical Searches	6	The existence of dark matter (DM) is well-established by gravitational observations across various distances, with no non-gravitational signals detected so far, see Ref. [1] for a recent review. On the one hand, such non-gravitational interactions of DM with the Standard Model (SM) are tightly constrained by direct and indirect detection searches. On the other hand, nightmare scenarios of strictly gravitational interactions would not explain the similarity of DM and SM abundances. These observations can be reconciled if a dark sector thermally interacted with the SM in the early universe before undergoing a phase transition that produced SM-singlet relics.	
C. Collider Searches	7	We show that this can occur in a broad class of confining dark sectors. We extend the SM by a sector of dark quarks charged under a confining $SU(N_c)$ that form an N_f -plet of SM $SU(2)_L$ with vanishing hypercharge, see <i>e.g.</i> Refs. [2–10] for previous studies of similar theories. The lightest dark baryons in the confined phase are stable and, if neutral, constitute a viable DM candidate. This is a simple DM scenario where the dark sector was in thermal contact with the SM in the early universe (without invoking an additional portal), while the degrees of freedom present today can have very feeble SM interactions, depending on the values of N_c and N_f .	
V. Conclusion and Outlook	7		
Acknowledgments	8		
A. Modifications to the $SU(2)_L$ Running Coupling	9		
B. Further Details on Hadron Representations	10		
1. Spin and Flavor Representations	10		
2. Finding Hadron Wavefunctions and $SU(2)_L$ Representations	11		
3. More Insights on the $SU(N_f) \rightarrow SU(2)_L$ Decomposition	16		

*Email: pasadi@uoregon.edu

†Email: abatz@uoregon.edu

‡Email: kribs@uoregon.edu

In the deconfined phase of the theory, this model contains ingredients similar to the standard Weakly Interacting Massive Particle (WIMP), with the addition of a dark confining gauge group. In the confined phase of the theory, the dark quarks assemble into dark hadrons, including a WIMP-like dark baryon DM candidate. Similar to a vanilla WIMP model, the dark baryons transform in particular representations of $SU(2)_L$. Unlike a vanilla WIMP model, we remain agnostic to the mechanism that fixes the DM relic abundance in the early universe, focusing on the prospects of different discovery channels today.

Regardless of N_c and N_f , the DM candidate has suppressed electromagnetic interactions with SM due to \mathcal{H} -parity [10]. This symmetry forbids the leading electromagnetic moments of the dark sector’s neutral hadrons, which strongly suppresses direct detection signals in our model. Therefore, the leading direct detection signals arise from electroweak loop-induced interactions due to the renormalizable interactions of the dark baryons with the W gauge boson [11–19]. For baryons in the singlet representation of $SU(2)_L$, these interactions vanish as well.

We study the $SU(2)_L$ representations of dark baryons for various combinations of N_c and N_f using standard group theory arguments. In the specific case where $N_f = 2$ and N_c is even, the lightest dark baryon is a pure singlet,¹ and the interactions with the SM become highly suppressed.² For many other combinations of N_c and N_f , we find that the DM state is composed primarily of a singlet of $SU(2)_L$ with only a small mixing with non-singlet dark baryons, so the elastic scattering rate relevant to direct detection signals of these models is suppressed by this small mixing. These (approximate) singlet baryons are inert composites of charged constituents, analogous to noble gases, so we have named them Noble Dark Matter.

Despite confining dark sectors being targets of different search strategies, *e.g.* see Refs. [2, 5, 7, 8, 19–59], our results imply that even this simplest confining extension of the WIMP paradigm is far more elusive than historically appreciated (see also Ref. [60] for non-confining WIMPs that are notoriously difficult to detect). Confinement in the dark sector naturally gives rise to a rich spectrum of WIMP-like states in the infrared (IR) despite including only one set of dark quarks in the ultraviolet (UV) that transform in a vector-like representation of the electroweak and the dark gauge groups. The effective field theory (EFT) in the IR inherits symmetries from the UV, particularly \mathcal{H} -parity, that forbid some interactions between the dark sector and the SM. The UV

theory also predicts other mechanisms that suppress interactions between the SM and the dark sector in the IR (*i.e.* singlets with small mixings with other states) that may appear unnatural or contrived from a bottom-up perspective. Earlier simplified model approaches introducing a single (possibly composite) electroweak multiplet have neglected this possibility.

The structure of the paper is as follows: In Sec. II, we introduce our model, review \mathcal{H} -parity, and explain baryon $SU(2)_L$ representations. We compute the lowest-lying baryon mass spectra and mixings of states in different $SU(2)_L$ representations for two $N_{c,f}$ combinations in Sec. III using the non-relativistic quark model, including electroweak contributions. We find that the DM candidate in these examples is mostly made of an $SU(2)_L$ singlet state and discuss in Sec. IV the resulting suppression of (in)direct detection signals, motivating searches at current and future high-energy colliders. We conclude in Sec. V. In App. A, we study the effect of the new fields on the running of $SU(2)_L$ gauge coupling. Further details on group theory arguments relevant for determining the $SU(2)_L$ representations and wavefunctions of dark baryons are provided in App. B. We also discuss details of a variation method used in determining the baryon mass spectrum in App. C.

II. THE THEORY

A. \mathcal{H} -parity from the Ultraviolet

We propose a theory of dark matter that arises from a new strongly-coupled confining gauge sector with the Lagrangian

$$\mathcal{L}_{\text{dark}} = -\frac{1}{4}G^{\mu\nu a}G_{\mu\nu}^a + \bar{\mathbf{Q}}(i\not{D} - m_0)\mathbf{Q}, \quad (1)$$

where $G_{\mu\nu}^a$ is the field strength of the dark $SU(N_c)$ with confinement scale Λ_χ and coupling α_χ , and \mathbf{Q} is a vector-like dark quark with bare mass m_0 that transforms as a fundamental of $SU(N_c)$ and an N_f -plet of $SU(2)_L$.³ In the confined phase of the theory, dark quarks bind into mesons and baryons. Since $\mathcal{L}_{\text{dark}}$ includes no hypercharge interactions, each quark or hadron in the dark sector has an electric charge equal to its weak isospin.

The lightest baryon in the confined phase is stabilized by a $U(1)_{\text{baryon}}$ in the standard way. If this baryon is neutral, it can be a viable DM candidate. As shown in Ref. [10], electromagnetic moments of the neutral dark baryons are strongly suppressed because they are eigenstates of the \mathcal{H} -parity transformation (where the electroweak gauge fields are charge-conjugated and $\mathbf{Q} \rightarrow$

¹ By “singlet”, we refer specifically to a state transforming in the trivial representation of $SU(2)_L$. Neutral components of non-trivial $SU(2)_L$ multiplets are referred to as such.

² The leading interaction is the electromagnetic polarizability of the composite singlet.

³ The added matter content can spoil the asymptotic freedom of $SU(2)_L$. See App. A for a discussion of Landau poles.

$e^{i\pi J_y} \mathbf{Q}$, with J_y the second generator of $SU(2)_L$. In the upcoming sections, we discuss the baryons' $SU(2)_L$ representations and mass spectrum, as well as the phenomenological implications of our findings. The vanishing of baryon electromagnetic moments and the spectrum of $SU(2)_L$ representations have a strong impact on possible experimental signatures.

B. Baryon Representations in the Infrared

In the confined phase of the theory, hadron states can be organized into multiplets transforming in irreducible representations of $SU(2)_L$. Baryon wavefunctions can be thought of as multi-particle states of identical fermions tracking each particle's position, dark color, flavor, and spin. For symmetric spatial states and anti-symmetric ($SU(N_c)$ -singlet) color states, the required constituent exchange symmetry of baryon spin-flavor wavefunctions restricts baryon states to those in specific flavor representations of $SU(N_f)$. In particular, the allowed flavor representations of $SU(N_f)$ have a corresponding $SU(2)_{\text{spin}}$ representation with an identical Young tableau. These tableaux have the form

$$\begin{array}{c} \boxed{} \cdots \boxed{} \boxed{} \cdots \boxed{} \\ \boxed{} \cdots \boxed{} \underbrace{ \cdots }_{2S} \\ \underbrace{ \cdots }_{N_c/2 - S} \end{array} \quad (2)$$

for spin- S baryons because N_c dark quarks are combined to make a color-singlet baryon, and the tableau for a spin- S representation of $SU(2)_{\text{spin}}$ has at most two boxes in each column and $2S$ columns with one box. See App. B1 for more details.

Enumerating the dark baryons' $SU(2)_L$ representations amounts to decomposing the $SU(N_f)$ representation in Eq. (2) into representations of its gauged $SU(2)$ subgroup. We explain the derivation of these decompositions and hadron spin-flavor wavefunctions in App. B2.

In the electroweak-broken phase, states in different $SU(2)_L$ representations can mix. However, neutral baryons in adjacent odd representations have opposite charges under \mathcal{H} -parity [10], which forbids their mixing. For example, a singlet can mix with the neutral components of 5-plets, 9-plets, *etc.* (\mathcal{H} -parity even), while it cannot mix with neutral components of 3-plets, 7-plets, *etc.* (\mathcal{H} -parity odd).

In Table I, we show the $SU(2)_L$ representations of all lowest-spin and spatially symmetric baryons for each set of $N_{c,f} = 2, \dots, 5$ (see App. B3 for more). Note the appearance of $SU(2)_L$ singlets, as states composed of singlets will have important implications for dark matter interactions, as we will see. We can classify the theory

(N_c, N_f)	Baryon $SU(2)_L$ Representations	Category
(2,2)	1	I
(2,3)	3	III
(2,4)	5 ⊕ 1	II
(2,5)	7 ⊕ 3	III
(3,2)	2	IV
(3,3)	5 ⊕ 3	III
(3,4)	8 ⊕ 6 ⊕ 4 ⊕ 2	IV
(3,5)	11 ⊕ 9 ⊕ 7 ⊕ 5 ⊕ 3	III
(4,2)	1	I
(4,3)	5 ⊕ 1	II
(4,4)	9 ⊕ 5 ⊕ 5 ⊕ 1	II
(4,5)	13 ⊕ 9 ⊕ 9 ⊕ 7 ⊕ 5 ⊕ 5 ⊕ 1 ⊕ 1	II
(5,2)	2	IV
(5,3)	7 ⊕ 5 ⊕ 3	III
(5,4)	12 ⊕ 10 ⊕ 8 ⊕ 8 ⊕ 6 ⊕ 6 ⊕ 4 ⊕ 4 ⊕ 2	IV
(5,5)	17 ⊕ 15 ⊕ 13 ⊕ 13 ⊕ 11 ⊕ 11 ⊕ 11 ⊕ 9 ⊕ 9 ⊕ 9 ⊕ 9 ⊕ 7 ⊕ 7 ⊕ 7 ⊕ 5 ⊕ 5 ⊕ 5 ⊕ 5 ⊕ 3 ⊕ 3 ⊕ 1	II

TABLE I: $SU(2)_L$ representations of the lowest-spin dark baryons in the confined phase of the model in Eq. (1) for several combinations of number of dark colors N_c and flavors N_f . We define in the text the four categories in the rightmost column describing when singlets and other neutral states appear.

space into four categories:⁴

- I. When N_c is even and $N_f = 2$, the lowest-spin baryon spectrum includes only a singlet of $SU(2)_L$, as one can infer from Eq. (2).
- II. One or more singlets are accompanied by non-trivial odd representations of $SU(2)_L$. The lightest state in the spectrum can be a mixture of the singlet and other neutral states.
- III. There are no singlets, and instead only non-trivial odd representations of $SU(2)_L$. The lightest baryon may be neutral, but it must transform non-trivially under $SU(2)_L$.
- IV. When N_c is odd and N_f is even, the baryons are in even representations of $SU(2)_L$, so none of them are neutral.

We discuss the phenomenology of prospective DM candidates corresponding to each category in Sec. IV. As we

⁴ Analogous categories exist when the quarks are spin-0, and singlets appear with similar frequency. See App. B4.

will explain, categories I and II are particularly interesting to us.

III. MASSES IN THE HEAVY QUARK LIMIT

Our DM candidate is the lightest mass eigenstate in the dark baryon spectrum. To identify which baryon state is the lightest, we use the non-relativistic quark model in the heavy quark limit, where hadrons are well-approximated as weakly-coupled bound states of their valence quarks [61–63]. We discuss the mass Hamiltonian in this limit and our approximation of its ground state using the variational method. We focus on the models with $(N_c, N_f) = (2, 4)$ and $(4, 3)$, as these are the simplest cases in category II defined in Sec. II B (where the baryon spectra include singlets among neutral states in non-trivial $SU(2)_L$ multiplets).

A. Electroweak Contributions in the Quark Model

Including leading-order $SU(N_c)$ and electroweak effects, the spatially-symmetric baryon mass is given by the operator (derived in App. C1) [64]

$$M = \sum_i \left(m_i + \frac{\langle p_i^2 \rangle}{2m_i} \right) + \sum_{i<j} \langle V_{ij}^X + V_{ij}^{\text{EM}} + V_{ij}^Z + V_{ij}^W \rangle + \mathcal{O}(p_{i,j}^3/m_q^3), \quad (3)$$

$$\langle V_{ij}^X \rangle = -\alpha_X \frac{N_c + 1}{2N_c} \mathcal{V}(0) + \mathcal{O}(\alpha_X^2),$$

$$\langle V_{ij}^{\text{EM}} \rangle = \alpha_{\text{EM}} Q_i Q_j \mathcal{V}(0) + \mathcal{O}(\alpha_{\text{EM}}^2),$$

$$\langle V_{ij}^Z \rangle = \alpha_W \cos^2 \theta_W Q_i Q_j \mathcal{V}(m_Z) + \mathcal{O}(\alpha_W^2),$$

$$\langle V_{ij}^W \rangle = \frac{\alpha_W}{2} \left(J_+^i J_-^j + J_-^i J_+^j \right) \mathcal{V}(m_W) + \mathcal{O}(\alpha_W^2),$$

$$\begin{aligned} \mathcal{V}(m_V) = & a_1 + \frac{1}{4m_q^2} \left(1 + \frac{8}{3} \mathbf{S}_i \cdot \mathbf{S}_j \right) (m_V^2 a_1 - 4\pi\delta) \\ & + \frac{m_V}{8m_q^2} (m_V^2 a_0 - 6m_V a_1 + 4a_2) \\ & - \frac{1}{4m_q^2} (m_V^2 c_1 - 4m_V c_2 - 2b + m_V d_2 - 2d_3), \end{aligned}$$

where sums are over constituents in the i^{th} position of the spin-flavor wavefunction with masses m_i , momenta \mathbf{p}_i , spins \mathbf{S}_i , and charges Q_i . The inter-quark potential has terms from exchange of a dark gluon (V_{ij}^X), photon (V_{ij}^{EM}), and weak bosons ($V_{ij}^{W,Z}$). The electromagnetic and $SU(2)_L$ couplings α_{EM} and α_W appear, as well as the Weinberg angle θ_W . J_{\pm}^i are $SU(2)_L$ ladder operators acting on the i^{th} constituent (see App. B2 for explicit forms). Expectation values $\langle \cdot \rangle$ in Eq. (3) are taken with respect to spatial wavefunctions, so M is an operator that acts on baryon spin-flavor states. The mass

m_q is the common tree-level mass of the quarks, which is distinct from m_i due to self-energy corrections inducing quark mass splittings (see App. C2). The function \mathcal{V} depends on the vector boson mass m_V and various spatial expectation values, written in the position basis as

$$\begin{aligned} a_n &= \langle r^{-n} e^{-m_V r} \rangle, \\ b &= \langle r^{-1} e^{-m_V r} \nabla_i \cdot \nabla_j \rangle, \\ c_n &= \langle r^{-n} e^{-m_V r} \mathbf{r} \cdot (\nabla_i - \nabla_j) \rangle, \\ d_n &= \langle r^{-n} e^{-m_V r} \mathbf{r} \cdot (\mathbf{r} \cdot \nabla_i) \nabla_j \rangle, \\ \delta &= \langle \delta^{(3)}(\mathbf{r}) \rangle, \end{aligned} \quad (4)$$

with $\mathbf{r} = \mathbf{r}_i - \mathbf{r}_j$ the inter-quark separation and ∇_i the gradient with respect to \mathbf{r}_i . The potential is a generalization of the well-known Fermi-Breit potential (used in Ref. [61] for the electromagnetic and strong potentials in the SM) to include effects of the W and Z masses $m_{W,Z}$.

The W and Z potentials include contact terms (with the δ factor) that are unsuppressed in the limit $m_q/m_V \rightarrow 0$. These terms are essential for M to be consistent with gauge invariance in the limit $m_{W,Z} \rightarrow 0$, as explained in App. C3. Also, new terms arise in the finite- $m_{W,Z}$ regime that are not present in the usual Fermi-Breit potential for massless vector boson exchange [64]. We must account for both of these effects to accurately capture the mass splittings induced by differences among baryon spin-flavor matrix elements of operators with $Q_i Q_j$ and $J_{\pm}^i J_{\mp}^j$.

There are two physically-relevant bases in which we express baryon states: the $SU(2)_L$ basis and the mass basis. In the $SU(2)_L$ basis, each state is a component of a multiplet that transforms in a well-defined irreducible representation of $SU(2)_L$. We express the mass operator in Eq. (3) in the $SU(2)_L$ basis, then diagonalize it to transform to the mass basis. In this way, we can express a baryon mass eigenstate as a linear combination of states with well-defined SM interactions.

B. Mass Spectra from the Variational Method

To estimate the spatial expectation values in Eq. (4), we use the variational method with the following template spatial wavefunction:

$$\psi = \left(1 + k_1 \sum_{i<j} |\mathbf{r}_i - \mathbf{r}_j| \right) e^{-k \sum_{i<j} |\mathbf{r}_i - \mathbf{r}_j|}, \quad (5)$$

where k and k_1 are optimization parameters with respect to which we minimize mass eigenvalues. The function is symmetric in the exchange of constituents, as we are interested in the lowest-lying (s -wave) hadrons. Similar template functions were used in Ref. [6], and an overall exponential suppression is typical in other weakly-bound

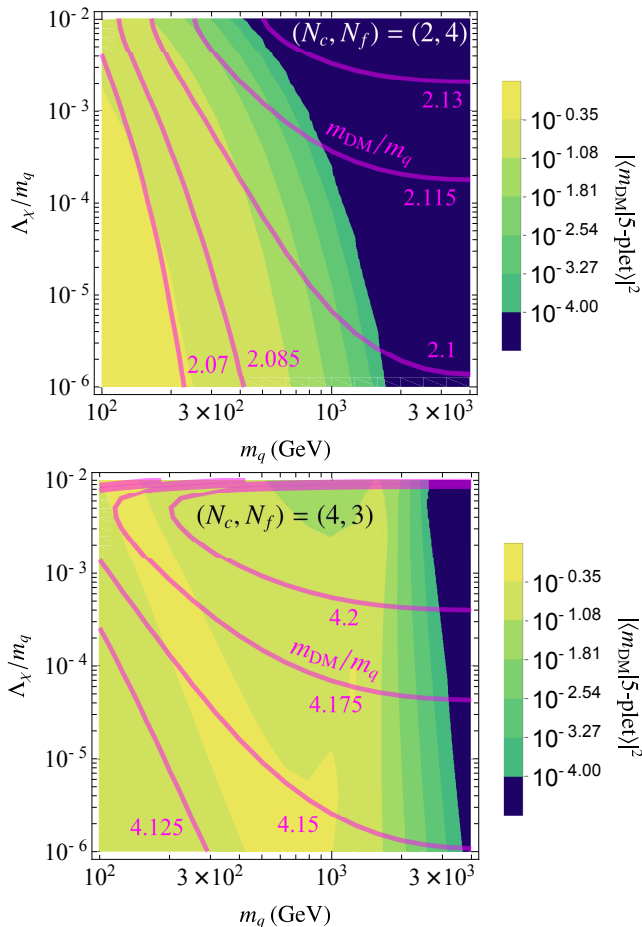


FIG. 1: Mass m_{DM} of the lightest baryon and overlap of the lightest mass eigenstate $|m_{\text{DM}}\rangle$ with the neutral $\text{SU}(2)_L$ 5-plet state $|5\text{-plet}\rangle$ for $(N_c, N_f) = (2, 4)$ (**top**) and $(4, 3)$ (**bottom**), which are two benchmark models from category II in Sec. II B. As the dark quark mass m_q increases, DM’s overlap with the non-singlet state decreases. DM masses are slightly greater than $N_c m_q$ due to quark self-energy corrections.

states such as atoms. Further details on how we compute the spatial expectation values are in App. C 4.

We show the masses of the lightest neutral baryons and their overlaps with the $\text{SU}(2)_L$ 5-plet states in Fig. 1 for $(N_c, N_f) = (2, 4)$ and $(4, 3)$. In the full parameter space shown, the lightest baryons are neutral and therefore may be viable DM candidates. The numerous terms in Eq. (3), each with different dependence on m_q and Λ_χ , give rise to non-trivial features in the mixing contours.

We verified that our calculation satisfies various consistency checks. For example, the quark-level calculation should reproduce expectations from hadron-level self-energy corrections. In particular, charged hadrons should typically be heavier than neutral hadrons, and hadron states in $\text{SU}(2)_L$ representations with larger Casimir factors should have a larger overlap with heavier mass eigenstates. Indeed, we find that the lightest baryon is neutral in the full parameter space shown, and the 5-plet has

larger overlap with heavier mass eigenstates than the singlet. The heavier neutral mass eigenstate can be heavier than the singly-charged state in the small- m_q region due to quark mass splittings or differences in electroweak matrix elements. See App. C 3 for elaboration.

In our numerical evaluation of the mass spectrum, we verified that in the limit of $m_q, \Lambda_\chi \gg m_{W,Z}$, the mixing between the singlet and the neutral component of the 5-plet vanish, as expected. In the large- m_q regime, we find the mass splittings between the heavier neutral and singly-charged baryons to be $\mathcal{O}(10^2)$ MeV, which is very close to the 166 MeV expectation for the mass splitting of any heavy singly-charged and neutral component of an $\text{SU}(2)_L$ multiplet [65].

IV. PHENOMENOLOGY

In this section, we discuss the phenomenology of our Noble Dark Matter in different contexts. In particular, we highlight their elusiveness in direct detection experiments, while also commenting on possible collider and astrophysical signatures.

A. Direct Detection

As first described in Ref. [10], \mathcal{H} -parity forbids leading electromagnetic moments of neutral hadrons in our model for all $N_{c,f}$ values, and thus significantly reduces the cross section of \mathcal{H} -parity-symmetric DM with the SM. Therefore, as with WIMPs, electroweak loop-induced interactions become the dominant source of direct detection signal [11–19]. The strength of these interactions strongly depends on the lightest baryon’s representation under $\text{SU}(2)_L$, giving rise to different phenomenology in each of the four categories defined in Sec. II B. Below, we discuss the direct detection signal of each category.

- I. DM is a pure $\text{SU}(2)_L$ singlet,⁵ so it does not have renormalizable interactions with electroweak gauge bosons. This is nearly a direct detection nightmare scenario.⁶
- II. DM can be a mixture of the singlet and other neutral states, as shown in Fig. 1 for $(N_c, N_f) = (2, 4)$ and $(4, 3)$. Electroweak loop-induced signals are suppressed by this mixing, as explored below.
- III. DM can be a mixture of neutral states in different non-trivial $\text{SU}(2)_L$ multiplets, and their interfering

⁵ For the specific case of $N_{c,f} = 2$, it is shown that bound states of dark baryons can be stable and constitute a fraction of DM [49, 66].

⁶ The leading direct detection signal becomes polarizability, to which foreseeable experiments are insensitive for DM masses $> \mathcal{O}(100)$ GeV [10].

electroweak loop-induced interactions would need to be calculated carefully. In the special case where there is only one multiplet, or if the mixing of the lightest state with neutral states in other multiplets is forbidden by \mathcal{H} -parity,⁷ then DM has well-defined non-trivial interactions with the W (similar to the standard WIMP).

IV. When there are no neutral baryons, there is no viable single-baryon DM candidate. We do not discuss this category further in this work.

To constrain categories II and III with direct detection experiments, one should first identify the lightest mass eigenstate, verify it is neutral, and compute its composition of states in each $SU(2)_L$ representation. In the heavy quark limit, this can be carried out with the variational method we proposed in Sec. III.

In Fig. 2, we illustrate the effect of mixings in category II by estimating the direct detection cross sections for benchmark models $(N_c, N_f) = (2, 4)$ and $(4, 3)$, with $\Lambda_\chi/m_q = 10^{-2}$ and 10^{-6} . We use cross sections computed in Ref. [18] for a pure 5-plet WIMP, scaling the pure 5-plet cross sections by the overlap of the $|5\text{-plet}\rangle$ state with the lightest mass eigenstate $|m_{\text{DM}}\rangle$. The uncertainty bands in Fig. 2 are inherited from uncertainties in the calculation of Ref. [18] due to *e.g.* non-perturbative nuclear matrix elements. At sufficiently small masses, the DM candidate may be excluded by existing [67] or projected [68] constraints, or by future experiments probing down to the neutrino fog. As expected from Fig. 1, for sufficiently high DM masses (*i.e.* where $SU(2)_L$ appears unbroken) the cross section drops rapidly as the mixing between the DM and the 5-plet states approaches zero. For the parameters shown in the figure, the cross sections are suppressed below the neutrino fog for $m_{\text{DM}} \gtrsim \mathcal{O}(0.1 - 1)$ TeV, requiring new techniques for probing heavier DM masses in future direct detection experiments, see *e.g.* Refs. [69, 70].⁸

The effect of uncertainties in the cross section is most evident in the $(4, 3)$ model with $\Lambda_\chi/m_q = 10^{-6}$. In this case, Fig. 2 suggests the reach of future experiments that can probe down to the neutrino fog can vary from below 300 GeV to ~ 5 TeV, depending on the uncertainties. This large range of possibilities warrants a more precise calculation of the cross sections applicable to a wider range of DM masses in future work.

As noted in Ref. [10], the dimension-7 polarizability operators of our dark baryons are not forbidden by \mathcal{H} -parity and can give rise to scattering in direct detection

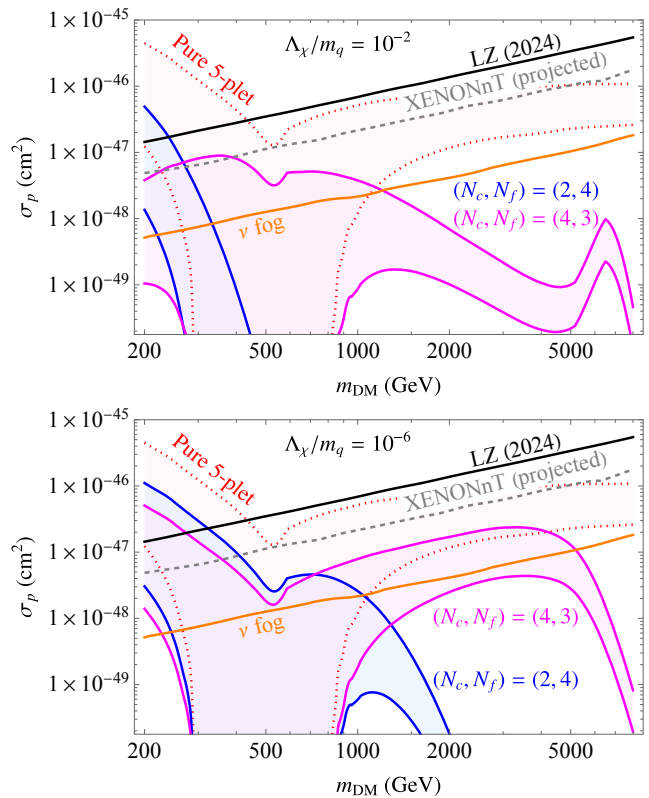


FIG. 2: Rough estimates of direct detection cross sections of the lightest dark baryon for $(N_c, N_f) = (2, 4)$ and $(4, 3)$ with $\Lambda_\chi/m_q = 10^{-2}$ (top) and 10^{-6} (bottom). We scaled the $SU(2)_L$ 5-plet cross sections (red dotted line) computed in Ref. [18] using a similar 5-plet WIMP model by $|\langle m_{\text{DM}} | 5\text{-plet} \rangle|^4$ for each $N_{c,f}$. The suppression of cross sections below the neutrino fog limits the reach of future experiments.

experiments, even when DM is a singlet of $SU(2)_L$. The cross section from these operators suffers from large uncertainties [75, 76] and is at best detectable in the current experiments for DM masses below a few hundred GeV. Future searches will not improve current bounds owing to the rapid drop in the cross section as a function of DM mass ($\sigma \propto 1/m_{\text{DM}}^6$). We have also checked numerically that in the large DM mass limit, the electroweak loop-induced interactions scale as $\sigma \propto 1/m_{\text{DM}}^4$. Therefore, the polarizability interaction is subdominant despite the small mixing.

We expect in general that other DM candidates in category II will be mostly comprised of singlet states with similarly small mixings of states in larger representations as in the two examples above. Therefore, we call the DM candidates in categories I and II Noble Dark Matter.

B. Indirect Detection and Astrophysical Searches

As for indirect detection, note that in the heavy quark limit, for the DM masses shown in Fig. 2, the symmetric

⁷ An example of this case is $(N_c, N_f) = (3, 3)$ (studied in Ref. [10]). The lowest-spin baryon spectrum contains only a 3-plet and 5-plet (adjacent odd representations), so \mathcal{H} -parity forbids the mixing of the neutral components.

⁸ In these benchmark models, we also find that the mass splittings of our lightest baryons are far above the ~ 100 keV threshold required for inelastic direct detection signals [41, 42, 71–74].

dark baryon abundance is completely depleted during a 1st order confinement phase transition by the squeezeout mechanism [77–79]. Thus, when the phase transition is of the 1st order, which is anticipated to occur for $N_c > 2$ and $\Lambda_\chi/m_q \lesssim 10^{-2}$ [80–86], we would need to augment the model to generate an asymmetric DM abundance today.

Even in the asymmetric limit, DM can accumulate in the center of stars. This can occur if the DM has a large enough interaction with SM such that it can lose its kinetic energy and slow down to below the escape velocity of the object. This accumulation can result in an implosion of the star via formation of a dense core that eventually collapses into a black hole [87–100]. There remains some debate in the literature as to the applicability of these bounds in certain DM ranges or self-interaction rates [101–104], thus a detailed study of this signal in our model remains an interesting future direction.

It is also argued that in models where there is more than one stable dark particle (whether baryons or nuclei), dark nucleosynthesis processes can give rise to detectable indirect detection signals, even in the asymmetric DM limit [49]. While lattice studies have established the existence of stable nuclei for the case of $N_{c,f} = 2$ [66], further studies on other combinations of N_f and N_c would be needed to determine the relevance of dark nucleosynthesis in these theories. Such dark nucleosynthesis processes are enhanced if the DM interacts enough with SM to be captured in the core of different celestial bodies.

In the case where a symmetric abundance could arise, such as by going to larger values of Λ_χ/m_q or for $N_c = 2$ where the phase transition is of 2nd order, other indirect detection signals can exist for the model as well. For models in category II, there can be direct annihilation of dark baryons to the SM, but the rate is suppressed by the mixing with non-singlet representations as in direct detection. The leading indirect detection signal arises from dark baryons annihilating to dark sector glueballs and/or rearranging into mesons. These daughter hadrons may further decay to the SM. In particular, as many of these mesons can be long-lived [3], this annihilation signal may be detectable in celestial-body focused searches [105]. A thorough study of all these indirect detection signals, in either the symmetric or asymmetric abundance limit, is left for future work.

C. Collider Searches

Sufficiently high-energy collisions could produce mesons, baryons, or glueballs of the dark sector. Glueballs are the lightest hadrons when $\Lambda_\chi \ll m_q$, but they could only be produced (at one loop) via highly-suppressed dimension-8 operators unless we introduced an additional portal [23, 25]. If $\Lambda_\chi \lesssim \text{few GeV}$, the Z boson can decay to dark glueballs through a quark loop to three dark gluons. Future colliders may be able to probe this contribution to the invisible width of the Z .

See Refs. [106–108] for invisible Z decay studies at future colliders.

If kinematically accessible, dark mesons and baryons can be produced in colliders via electroweak processes. For example, charged hadrons can be pair-produced, and neutral vector hadrons can mix with the SM photon or Z before decaying [2, 8]. Mesons (being lighter than baryons for $N_c > 2$) would dominate signals, potentially including *e.g.* missing energy plus initial state radiation [109], heavy stable charged particles, displaced vertices, disappearing tracks [110–114], semi-visible jets [29, 115], emerging jets [28], tumblers [116], and quirks [22]. For the relevant mass ranges in Fig. 2, the center-of-mass energy of hard scattering processes in foreseeable colliders would be insufficient to produce the large dark hadron multiplicities required for soft bombs (SUEPs) [31, 37]. See Refs. [117–119] for reviews.

These signals depend on the lifetimes of mesons, which can span a large range due to an accidental symmetry [3]. If these signals can be tagged efficiently, and if the energy of hard interactions that produce dark quarks and gluons is large enough relative to the dark hadron masses such that a parton shower and jet formation take place within the dark sector, then energy-energy correlators could be used to probe the dark confining phase transition [120–122]. We leave a comprehensive study of all these collider signals for future work.

V. CONCLUSION AND OUTLOOK

We studied a sector with dark quarks transforming under a confining $SU(N_c)$ as well as an N_f -plet of $SU(2)_L$. We described a systematic way to determine dark baryon $SU(2)_L$ representations using Eq. (2) and showed that for various N_c, N_f combinations, there are one or more $SU(2)_L$ singlets in the lowest-spin baryon spectrum, see Table I. Using the non-relativistic quark model, we develop a variational method for calculating the baryon mass spectrum in the heavy quark limit, including the electroweak contributions in the inter-quark potential.

We found that the lightest baryons in these models are neutral and mostly overlap with the singlet states. For $m_q \gtrsim \mathcal{O}(1)$ TeV, the mixing of the DM candidate with the non-singlet state is significantly suppressed, as illustrated in Fig. 1. Thus, while the dark sector is in thermal contact with the SM in the early universe, the DM candidate in the hadronic phase has strongly suppressed interactions with SM today.

leading electromagnetic moments are forbidden by \mathcal{H} -parity [10], and electroweak loop-induced signals are suppressed when the the DM candidates are (approximate) $SU(2)_L$ singlets. It is remarkable that symmetries of the simple UV theory considered in this paper lead to a low energy effective theory of dark matter with such highly suppressed interactions.

We focused on the $(N_c, N_f) = (2, 4)$ and $(4, 3)$ baryon spectra because they have two neutral states (which are

permitted to mix by \mathcal{H} -parity), one of which is a singlet. The lowest-spin spectra of other $N_{c,f}$ combinations can contain only a singlet (category I from Table I), a singlet with more complicated mixing (category II), or no singlet with a nonetheless viable DM candidate (category III). Each of these possibilities warrants further investigation, and we have presented methods to estimate the mass spectra and mixings of states in different $SU(2)_L$ representations in the heavy quark limit. In the $m_q < \Lambda_\chi$ regime, the calculation is complicated by relativistic and non-perturbative corrections, but we expect our qualitative conclusions based on perturbative electroweak effects to hold true. In particular, states in each $SU(2)_L$ representation become approximate mass eigenstates for $m_q \gg m_W$, states in larger representations of $SU(2)_L$ tend to be heavier, and charged states tend to be heavier than neutral states.

There are various generalizations of the model in Eq. (1) that could alter the phenomenology. Adding additional quark generations, scalar quarks, or quarks in different $SU(N_c)$ representations would complicate the hadron spectrum while preserving \mathcal{H} -parity. One could also add additional portals (such as a Higgs portal) to facilitate production and decay of dark hadrons, including glueballs.

It is interesting to compare and contrast our model to theories with elementary WIMPs. It is well known that DM composed of the neutral component of a single non-trivial $SU(2)_L$ multiplet (such as Wino) has a large indirect detection signal [123–126] and is widely considered to be ruled out. In our composite realization, electroweak multiplets can naturally mix with singlet states. This implies that considering only individual electroweak multiplets in isolation may prematurely dismiss WIMP-like dark matter. Combinations of multiple WIMPs could have been considered in the context of an EFT of elementary states, but the mass hierarchy and mixings would be free parameters. We have seen that the IR description of a composite realization of electroweak multiplets provides the mass spectrum and the mixings as calculable outcomes of a simple UV theory. Therefore, there is a much larger theory space of WIMP-like dark matter with multiple states and associated mixings.

There are of course distinctions between elementary WIMPs and the composite WIMP-like states that we encounter in Nobel Dark Matter. For instance, in addition to the baryon states, there is also a set of meson states that are expected to be lighter than the baryons. The meson states are anticipated to have important implications for indirect detection (annihilation of dark baryons to dark mesons) as well as collider signals. We reserve a more thorough analysis of the rich phenomenology for future work.

Acknowledgments

We thank Elias Bernreuther, Tom Bouley, Marco Costa, Sam Homiller, Nick Rodd, and Tracy Slatyer for helpful discussions. This work is supported in part by the U.S. Department of Energy under grant number DE-SC0011640.

Appendix A: Modifications to the $SU(2)_L$ Running Coupling

The dark quark fields we introduce in Eq. (1) modify the β -function of α_W at scales above m_q . At sufficiently large N_c and N_f , the appearance of Landau poles necessitates a UV completion at a scale below where the coupling diverges [127]. At one loop and for renormalization scale $\mu > m_q$ [128],

$$\frac{1}{\alpha_W(\mu)} = \frac{1}{\alpha_W(m_q)} - \frac{\beta_0}{2\pi} \ln \frac{\mu}{m_q} \quad (\text{A1})$$

$$\simeq \frac{1}{\alpha_W(m_Z)} - \frac{\beta_{\text{SM}}}{2\pi} \ln \frac{m_q}{m_Z} - \frac{\beta_0}{2\pi} \ln \frac{\mu}{m_q}, \quad (\text{A2})$$

with

$$\beta_0 = \beta_{\text{SM}} + \frac{4}{3} T_R N_c \quad (\text{A3})$$

$$\beta_{\text{SM}} = -\frac{19}{6} \quad (\text{A4})$$

$$\text{Tr}(J_a J_b) = T_R \delta_{ab}, \quad a, b \in \{x, y, z\} \quad (\text{A5})$$

$$T_R = \frac{N_f(N_f^2 - 1)}{12}. \quad (\text{A6})$$

One obtains Eq. (A2) from Eq. (A1) by running α_W from $\mu = m_Z$ to $\mu = m_q$ with the SM field content.

The N_f^3 scaling of T_R quickly spoils the asymptotic freedom of $SU(2)_L$, as the β -function is negative only if $N_f = 2$ and $N_c \leq 4$. Otherwise, there is a UV Landau pole Λ_W where $1/\alpha_W(\Lambda_W) = 0$. Solving Eq. (A2) for Λ_W ,

$$\Lambda_W = m_q \left(\frac{m_Z}{m_q} \right)^{\beta_{\text{SM}}/\beta_0} \exp \left(\frac{2\pi}{\beta_0 \alpha_W(m_Z)} \right) \quad (\text{A7})$$

$$= m_q \left(\frac{m_Z}{m_q} \right)^{\frac{-57}{-57+2N_c N_f(N_f^2-1)}} \exp \left(\frac{36\pi}{(-57+2N_c N_f(N_f^2-1)) \alpha_W(m_Z)} \right). \quad (\text{A8})$$

As shown in Table A1, one quickly encounters sub-Planckian Landau poles ($\Lambda_W < M_{\text{Pl}} \sim 10^{19}$ GeV) for modest values of $N_{c,f}$. It was already noted in Ref. [10] that our model requires a UV completion below the Planck scale (perhaps even below the Grand Unification scale) to facilitate meson decays before Big Bang Nucleosynthesis, but the Landau poles imply that a UV completion is needed at an even lower scale for some N_c, N_f . When Λ_W/m_q is not very large (say $\lesssim 10^3$), one must carefully consider the effects of higher-dimensional operators induced by the UV completion. These effects can include baryon number violation, \mathcal{H} -parity violation, and large two-loop corrections to the SM $SU(3)_{\text{color}}$ and $U(1)_Y$ couplings. This pathology is particularly pronounced for $N_f \geq 5$, where Λ_W/m_q can be $\mathcal{O}(10)$.

(N_c, N_f)	Λ_W (GeV) for $m_q = 1$ TeV	Λ_W (GeV) for $m_q = 1$ PeV
(2,2)	—	—
(2,3)	10^{42}	10^{49}
(2,4)	10^{11}	10^{15}
(2,5)	10^6	10^{10}
(3,2)	—	—
(3,3)	10^{20}	10^{25}
(3,4)	10^8	10^{11}
(3,5)	10^5	10^8
(4,2)	—	—
(4,3)	10^{14}	10^{18}
(4,4)	10^6	10^{10}
(4,5)	10^4	10^8
(5,2)	10^{508}	10^{568}
(5,3)	10^{11}	10^{15}
(5,4)	10^6	10^9
(5,5)	10^4	10^7

TABLE A1: Order-of-magnitude estimates of $SU(2)_L$ Landau poles Λ_W for various $N_{c,f}$ combinations using Eq. (A8). Dashes indicate where $SU(2)_L$ remains asymptotically free. Some versions of the theory are safe from sub-Planckian Landau poles, and others require a UV completion at modestly high scales.

Appendix B: Further Details on Hadron Representations

Our conclusions about the phenomenology of the confining dark sector we present in Sec. II depend on the possible $SU(2)_L$ representations of the dark baryons, so we require a systematic approach to enumerate them for any combination of N_c and N_f . Future analyses of collider signals and cosmology would also benefit from understanding the meson spectrum and representations.

1. Spin and Flavor Representations

We employ the quark model [61–63], wherein hadron states are products of color, flavor, spin, and spatial wavefunctions. Baryon states with identical fermionic constituents must be totally anti-symmetric under particle exchange. Meson constituents transform in conjugate representations of their symmetry groups, so a multi-particle meson state does not consist of identical particles and therefore need not have definite exchange symmetry. Since we are most interested in the lightest hadrons, we restrict our analysis to states with vanishing orbital angular momentum and symmetric spatial wavefunctions, and we emphasize the lowest-spin states.

Under the assumption of confinement, hadron states transform in the singlet representation of $SU(N_c)$, which implies baryon color wavefunctions are totally anti-symmetric in exchange of their N_c constituents. With our additional assumption of even spatial wavefunctions, the combined spin-flavor states of the baryons in our model must be totally symmetric in particle exchange. Therefore, baryons with spin-1/2 constituents have spin-flavor states belonging to the symmetric representation of $SU(2N_f)$ with the Young tableau

$$\underbrace{\begin{array}{c} \square \cdots \square \\ \square \end{array}}_{N_c} \tag{B1}$$

$$\text{dimension} = \frac{(2N_f - 1 + N_c)!}{N_c! (2N_f - 1)!}.$$

The group is $SU(2N_f)$ since for each of the N_f possible flavors, there are two possible spin states. The dimension of this representation counts the number of baryon spin-flavor states, including all spin degrees of freedom. However,

since we want to understand the hadrons' $SU(2)_L$ representations, and $SU(2)_L$ is a subgroup of the $SU(N_f)$ flavor symmetry (analogous to SM isospin), it is useful to consider the hadron states' flavor representations in $SU(N_f)$ separately from their spin representations in $SU(2)_{\text{spin}}$.

In order for a baryon's combined spin-flavor representation to be totally symmetric, its representations in $SU(N_f)$ and $SU(2)_{\text{spin}}$ *must have identical exchange symmetries*. Therefore, those representations must have identical Young tableaux when written out with all N_c boxes. The tableaux for $SU(2)_{\text{spin}}$ representations have at most two boxes in each column, so the same is true for the relevant $SU(N_f)$ representations. Thus, spin- S baryon states belong to the flavor representation of $SU(N_f)$ with the tableau⁹

$$\begin{array}{c}
 \begin{array}{ccccccc}
 \square & \cdots & \square & \square & \cdots & \square & \\
 \square & \cdots & \square & \underbrace{\square \cdots \square}_{2S} & & & \\
 \hline
 & & \underbrace{\square \cdots \square}_{N_c/2 - S} & & & &
 \end{array} \\
 \text{dimension} = \frac{(2S+1)(N_f + N_c/2 + S - 1)! (N_f + N_c/2 - S - 2)!}{(N_f - 1)! (N_f - 2)! (N_c/2 + S + 1)! (N_c/2 - S)!},
 \end{array} \tag{B2}$$

and the dimension of this representation counts the number of spin- S baryons, see also Ref. [6] for similar results. Unlike the expression in Eq. (B1), this counting does not include all values of $S_z = -S, \dots, S$ for the various $|S S_z\rangle$ baryon spin states.

As an example of applying Eq. (B2), consider the model with $N_c = 5$ and $N_f = 4$. Naïvely, a candidate flavor representation of $SU(4)$ for spin-1/2 baryons would be

$$\begin{array}{cc}
 \square & \square \\
 \square & \\
 \square & \\
 \square &
 \end{array} \tag{B3}$$

which can be contracted to the fundamental representation of $SU(4)$. This may seem to suggest that baryon states can be constructed in the flavor representation in Eq. (B3) and the fundamental representation of $SU(2)_{\text{spin}}$. This is, however, not true because there is no representation of $SU(2)_{\text{spin}}$ with the Young tableau in Eq. (B3). Any spin configuration with $S = 1/2$ has different particle exchange symmetries than any flavor configuration in the above representation, so the combined spin-flavor representation would not be totally symmetric. The only flavor representation with spin-1/2 baryons in this model would be

$$\begin{array}{ccc}
 \square & \square & \square \\
 \square & \square &
 \end{array} \tag{B4}$$

which is a valid tableau for an $SU(2)_{\text{spin}}$ representation that can be contracted to the fundamental representation. This is a dimension-60 representation of the $SU(4)$ flavor group. In App. B2, we describe how to construct baryon spin-flavor wavefunctions using the symmetry of the full $SU(2N_f)$ representation. We then show in App. B3 how to construct the flavor part of the wavefunctions (more efficiently) using the symmetry structure of the flavor representation in Eq. (B2).

2. Finding Hadron Wavefunctions and $SU(2)_L$ Representations

Now that we have the flavor representations in $SU(N_f)$, we can formally understand why the baryon states are in specific $SU(2)_L$ multiplets. Recall that $SU(2)_L$ is a subgroup of $SU(N_f)$. For \mathcal{H} -parity symmetric models, we are interested in the embedding of $SU(2)_L$ in $SU(N_f)$ where one identifies the N_f -dimensional irreducible representation of $SU(2)_L$ with the fundamental representation of $SU(N_f)$. One can express the flavor representation in Eq. (B2) as a direct sum of irreducible $SU(2)_L$ representations corresponding to this embedding. This is the decomposition shown in Table I for several combinations of N_c and N_f and the lowest-spin baryons.

⁹ A spin- S representation of $SU(2)_{\text{spin}}$ has a row of $2S$ boxes in its Young tableau after contraction.

We have an algorithm for finding all hadron spin-flavor wavefunctions with a particular spin state, organizing the states into $SU(2)_L$ multiplets, and using the wavefunctions to compute the matrix elements needed for the mass calculation. For concreteness, we define a spin-flavor eigenstate as a simultaneous eigenstate of the spin operators S^2 and S_z as well as all flavor number operators (*i.e.* a spin-flavor eigenstate has definite quark flavor content). We likewise define an $SU(2)_L$ eigenstate as a simultaneous eigenstate of the quadratic Casimir operator J^2 and the third generator J_z of $SU(2)_L$. The eigenvalues of J_z are electric charges Q (as the dark sector particles have vanishing hypercharge), and the eigenvalues of J^2 are $J(J+1)$. The spectrum of J quantum numbers indicates the decomposition of the $SU(N_f)$ representation in Eq. (B2) into representations of $SU(2)_L$, and each eigenstate of J^2 belongs to a $(2J+1)$ -plet of $SU(2)_L$. Enumerating all of these states requires finding all appropriately symmetrized combinations of flavor and spin configurations, then expressing these in a basis that simultaneously diagonalizes S^2 , S_z , J^2 , and J_z . Our algorithm finds these states for either mesons or baryons, and we specify the differences in those cases below.

A schematic description of our algorithm is

1. Find a complete basis of constituent spin configurations for the desired hadron spin state.
2. Find a complete basis of flavor configurations for the hadrons with the “middlest” electric charge ($Q = 1/2$ when N_c is odd and N_f is even and $Q = 0$ otherwise).
3. Combine the spin and flavor eigenstates to obtain a complete basis of spin-flavor eigenstates with this charge. For baryons, symmetrize the states and eliminate linear dependence and overlap of the symmetrized states.
4. Transform the basis of spin-flavor eigenstates to a basis that diagonalizes J^2 of $SU(2)_L$. Deduce the spectrum of hadron $SU(2)_L$ multiplets from the eigenvalues of J^2 .
5. Apply the $SU(2)_L$ ladder operators to the eigenstates of J^2 with the middlest charge to find all other $SU(2)_L$ eigenstates in each multiplet.

We elaborate on each step below, including examples. We start with the middlest electric charge because all $SU(2)_L$ multiplets contain a state with this charge. One could alternatively start with the highest charge and repeatedly lower it to construct the multiplets. However, that approach is more complicated because there may be additional states with the lower charge that one would have to find. For example, in the $(N_c, N_f) = (5, 3)$ model, if one started with the $Q = 3$ state in the baryon 7-plet and lowered it to the $Q = 2$ state, one would need to find the $Q = 2$ state in the 5-plet, then do the same again for the $Q = 1$ states in the 5-plet and triplet. By contrast, by finding all the $Q = 0$ states and raising/lowering them to fill out the multiplets, one needs to find all states with a particular charge only once.

One must first specify the desired $|S S_z\rangle$ hadron spin state. One can then find a complete, orthonormal basis of constituent spin configurations for that state. For mesons with spin-1/2 constituents, this basis is the well-known spin singlet or triplet state, so we emphasize the baryon case. One can start with the highest-spin baryon state $|S = \frac{N_c}{2} S_z = \frac{N_c}{2}\rangle$ and repeatedly apply the lowering operator S_- until the state has the desired S_z . One now has a spin state in the multiplet corresponding to the totally symmetric $SU(2)_{\text{spin}}$ representation with dimension $N_c + 1$. Therefore, the state is composed of all basis state spin configurations with the desired S_z . One can use this basis to diagonalize the operator S^2 and isolate the eigenstates with the desired $S(S+1)$ eigenvalues. One now has a complete, orthonormal basis of constituent spin configurations with the desired hadron spin state.

As an illustrative example, consider the baryon spectrum in the model with $(N_c, N_f) = (4, 3)$. The flavor representations of the required form in Eq. (B2) are

$$\begin{array}{|c|c|} \hline \square & \square \\ \hline \square & \square \\ \hline \end{array}
 \quad
 \begin{array}{|c|c|c|} \hline \square & \square & \square \\ \hline \square & & \\ \hline \end{array}
 \quad
 \begin{array}{|c|c|c|c|} \hline \square & \square & \square & \square \\ \hline \square & \square & \square & \square \\ \hline \end{array}
 \tag{B5}$$

corresponding to spin-0, spin-1, and spin-2 baryons, respectively. Suppose we desire baryons in the spin state $|S = 0 S_z = 0\rangle$. One applies S_- to the highest-spin state $|\uparrow\uparrow\uparrow\rangle$ to find the basis of six states with $S_z = 0$, each with two spin-up and two spin-down quarks. After diagonalizing S^2 , one finds two states with $S = 0$. A (non-unique) orthonormal basis in which to write these states is

$$|s_1\rangle = \frac{1}{\sqrt{12}} (2|\uparrow\uparrow\downarrow\downarrow\rangle + 2|\downarrow\downarrow\uparrow\uparrow\rangle - |\uparrow\downarrow\uparrow\downarrow\rangle - |\downarrow\uparrow\downarrow\uparrow\rangle - |\uparrow\downarrow\downarrow\uparrow\rangle - |\downarrow\uparrow\uparrow\downarrow\rangle)
 \tag{B6}$$

$$|s_2\rangle = \frac{1}{2} (|\uparrow\downarrow\uparrow\downarrow\rangle - |\downarrow\uparrow\downarrow\uparrow\rangle + |\downarrow\uparrow\uparrow\downarrow\rangle - |\uparrow\downarrow\downarrow\uparrow\rangle).
 \tag{B7}$$

Note that $|s_1\rangle$ is symmetric in exchanges of the first pair and last pair of particles, and $|s_2\rangle$ is anti-symmetric in these exchanges.

Next, one needs a complete, orthonormal basis of flavor configurations with the middle charge, either $Q = 1/2$ or $Q = 0$. This can be done similarly to the spin configurations above. Starting with the highest-charge flavor state, one can generate the symmetric $SU(2)_L$ multiplet by repeatedly applying J_- , and the resulting state is a combination of all flavor configurations with the desired charge. Labeling quark flavors by their charge and labeling anti-quark flavors with charge $-Q$ as \bar{Q} , the $SU(2)_L$ generators act on baryon and meson flavor states as

$$J_z |Q_1, \dots, Q_{N_c}\rangle = \sum_{i=1}^{N_c} Q_i |Q_1, \dots, Q_{N_c}\rangle, \quad (\text{B8})$$

$$J_{\pm} |Q_1, \dots, Q_{N_c}\rangle = \sum_{i=1}^{N_c} \sqrt{\frac{N_f^2 - 1}{4} - Q_i(Q_i \pm 1)} |Q_1, \dots, Q_i \pm 1, \dots, Q_{N_c}\rangle, \quad (\text{B9})$$

$$J_z |Q_1, \bar{Q}_2\rangle = (Q_1 - Q_2) |Q_1, \bar{Q}_2\rangle, \quad (\text{B10})$$

$$J_{\pm} |Q_1, \bar{Q}_2\rangle = \sqrt{\frac{N_f^2 - 1}{4} - Q_1(Q_1 \pm 1)} |Q_1 \pm 1, \bar{Q}_2\rangle - \sqrt{\frac{N_f^2 - 1}{4} - Q_2(Q_2 \mp 1)} |Q_1, \bar{Q}_2 \mp 1\rangle. \quad (\text{B11})$$

We work in the convention with

$$J_{\pm} = J_x \pm iJ_y, \quad (\text{B12})$$

$$J^2 = J_z^2 + \frac{1}{2} (J_+ J_- + J_- J_+), \quad (\text{B13})$$

where J_x and J_y are the first and second generators of $SU(2)_L$, respectively.

In the example of the $(4, 3)$ model, we can label the quark flavors as $+, 0, -$, corresponding to positive, zero, and negative electric charges, respectively. The highest-charge state is $|++++\rangle$. After applying J_- , one finds the $Q = 0$ flavor configurations

$$|f_1\rangle = |0000\rangle \quad (\text{B14})$$

$$|f_2\rangle = |--++\rangle \quad (\text{B15})$$

$$|f_3\rangle = |-00+\rangle, \quad (\text{B16})$$

plus permutations. Note that $|f_1\rangle$ has more exchange symmetries than $|f_2\rangle$, which has more than $|f_3\rangle$.

Now that one has bases for the spin and flavor configurations, one can find the combined spin-flavor states. For meson states, these are simply the tensor products of each flavor configuration with the spin configuration identified above. However, baryon spin-flavor states must be symmetrized. To find all the needed baryon states, one can start by finding the tensor product state of each flavor configuration with each spin configuration. For each of these tensor product states, written with each particle p_1, \dots, p_{N_c} having some flavor and spin assignment, one then finds the symmetrized state

$$\sum_{\sigma \in \text{perms}(N_c)} |p_{\sigma(1)}, \dots, p_{\sigma(N_c)}\rangle, \quad (\text{B17})$$

where $\text{perms}(N_c)$ is the set of all permutations of N_c elements. Any valid baryon spin-flavor eigenstate must be some symmetrized product of a flavor content with a spin configuration, so the set of all states obtained using Eq. (B17) is an over-complete set from which a complete basis of baryon spin-flavor eigenstates can be extracted. One can iteratively construct an orthogonal basis $\{|b_1\rangle, \dots, |b_n\rangle\}$ of states that are linear combinations of non-orthogonal states in the set $\{|v_1\rangle, \dots, |v_n\rangle\}$ using the Gram-Schmidt process. One sets $|b_1\rangle = |v_1\rangle$, then $|b_n\rangle$ is constructed using the previously found $n - 1$ states as

$$|b_n\rangle = |v_n\rangle - \sum_{i=1}^{n-1} \frac{\langle b_i | v_n \rangle}{\langle b_i | b_i \rangle} |b_i\rangle. \quad (\text{B18})$$

Since the original set of symmetrized baryon states is over-complete, some of the states constructed in this way will have zero norm, and such states can be discarded. One now has a complete, orthogonal basis of meson or baryon spin-flavor eigenstates with the desired spin and the middle charge.

In the (4, 3) model, symmetrizing the tensor product of the $|f_1\rangle$ flavor configuration with either spin configuration results in the state with zero norm. This is unsurprising, as $|f_1\rangle$ is totally symmetric in particle exchange, while neither spin configuration is totally symmetric. This case is analogous to the lack of a spin-1/2 baryon with three up quarks in the SM.

Finding the product of $|f_2\rangle$ with either spin state and symmetrizing gives the neutral baryon spin-flavor eigenstate

$$|\mathcal{B}_1^0\rangle = \frac{1}{\sqrt{72}}|--++\rangle \otimes (2|\uparrow\uparrow\downarrow\downarrow\rangle + 2|\downarrow\downarrow\uparrow\uparrow\rangle - |\uparrow\downarrow\uparrow\downarrow\rangle - |\downarrow\uparrow\downarrow\uparrow\rangle - |\uparrow\downarrow\downarrow\uparrow\rangle - |\downarrow\uparrow\uparrow\downarrow\rangle) + \text{perms}, \quad (\text{B19})$$

where ‘perms’ denotes particle permutations that do not return the same configuration. Doing the same with $|f_3\rangle$ results in

$$|\mathcal{B}_2^0\rangle = \frac{1}{12}|00+\rangle \otimes (|\uparrow\uparrow\downarrow\downarrow\rangle + |\downarrow\downarrow\uparrow\uparrow\rangle + |\uparrow\downarrow\uparrow\downarrow\rangle + |\downarrow\uparrow\downarrow\uparrow\rangle - 2|\uparrow\downarrow\downarrow\uparrow\rangle - 2|\downarrow\uparrow\uparrow\downarrow\rangle) + \text{perms}. \quad (\text{B20})$$

These form a complete basis of neutral baryons with the desired spin, but our algorithm prescribes also finding the symmetrized baryon states generated by the permuted flavor configurations not shown above to ensure all baryons are found. The Gram-Schmidt process eliminates the redundancy from pairing flavor and spin states that provide linearly dependent symmetrized baryon states.

One can determine the spectrum of hadron $\text{SU}(2)_L$ multiplets by using the basis of spin-flavor eigenstates to diagonalize the J^2 operator. These multiplets provide the decomposition of the $\text{SU}(N_f)$ flavor representation into irreducible representations of $\text{SU}(2)_L$. Some eigenvalues of J^2 may be degenerate (*e.g.* the scalar singlets for $(N_c, N_f) = (4, 5)$), in which case there is not a unique way to write the $\text{SU}(2)_L$ eigenstates as linear combinations of spin-flavor eigenstates.

Finally, one can repeatedly apply the J_{\pm} operators to the $\text{SU}(2)_L$ eigenstates with the middle charge to obtain the spin-flavor wavefunctions for all entries of each multiplet. One now has the full spectrum of lowest-lying hadron spin-flavor states with the desired spin, organized by $\text{SU}(2)_L$ representation and charge.

For the (4, 3) model, using the states in Eqs. (B19) and (B20) to diagonalize J^2 shows that the linear combination

$$|\mathcal{J}_0^0\rangle = -\frac{1}{\sqrt{3}}|\mathcal{B}_1^0\rangle + \sqrt{\frac{2}{3}}|\mathcal{B}_2^0\rangle \quad (\text{B21})$$

is an $\text{SU}(2)_L$ singlet, and acting with J_{\pm} on the orthogonal combination generates the $\text{SU}(2)_L$ 5-plet

$$\begin{pmatrix} |\mathcal{J}_2^{++}\rangle \\ |\mathcal{J}_2^{+}\rangle \\ |\mathcal{J}_2^0\rangle \\ |\mathcal{J}_2^{-}\rangle \\ |\mathcal{J}_2^{--}\rangle \end{pmatrix} = \begin{pmatrix} |\mathcal{B}^{++}\rangle \\ |\mathcal{B}^{+}\rangle \\ \sqrt{\frac{2}{3}}|\mathcal{B}_1^0\rangle + \frac{1}{\sqrt{3}}|\mathcal{B}_2^0\rangle \\ |\mathcal{B}^{-}\rangle \\ |\mathcal{B}^{--}\rangle \end{pmatrix}, \quad (\text{B22})$$

where

$$|\mathcal{B}^{++}\rangle = \frac{1}{\sqrt{72}}|00++\rangle \otimes (2|\uparrow\uparrow\downarrow\downarrow\rangle + 2|\downarrow\downarrow\uparrow\uparrow\rangle - |\uparrow\downarrow\uparrow\downarrow\rangle - |\downarrow\uparrow\downarrow\uparrow\rangle - |\uparrow\downarrow\downarrow\uparrow\rangle - |\downarrow\uparrow\uparrow\downarrow\rangle) + \text{perms} \quad (\text{B23})$$

$$|\mathcal{B}^{+}\rangle = \frac{1}{12}|0+0+\rangle \otimes (2|\uparrow\uparrow\downarrow\downarrow\rangle + 2|\downarrow\downarrow\uparrow\uparrow\rangle - |\uparrow\downarrow\uparrow\downarrow\rangle - |\downarrow\uparrow\downarrow\uparrow\rangle - |\uparrow\downarrow\downarrow\uparrow\rangle - |\downarrow\uparrow\uparrow\downarrow\rangle) + \text{perms}, \quad (\text{B24})$$

and the negatively-charged states $|\mathcal{B}^{-}\rangle$ and $|\mathcal{B}^{--}\rangle$ can be found by negating the flavors of the positively-charged states. In the above notation, states labeled with \mathcal{B} are spin-flavor eigenstates. States labeled with \mathcal{J} are $\text{SU}(2)_L$ eigenstates whose subscripts denote the J quantum numbers corresponding to the $J(J+1)$ eigenvalues of J^2 . The presence of the singlet and 5-plet shows that for the relevant embedding, the $\text{SU}(3)$ flavor representation decomposes to $\text{SU}(2)_L$ representations as

$$\text{SU}(3) \supset \text{SU}(2)_L \quad (\text{B25})$$

$$\begin{array}{|c|c|} \hline \square & \square \\ \hline \square & \square \\ \hline \end{array} \rightarrow \mathbf{5} \oplus \mathbf{1},$$

as stated in Table I.

Our other main example in Sec. III B is the $(N_c, N_f) = (2, 4)$ model, for which we briefly walk through the baryon wavefunction derivation here. The $\text{SU}(4)$ flavor representations are

$$\begin{array}{|c|} \hline \square \\ \hline \square \\ \hline \end{array} \quad \begin{array}{|c|c|} \hline \square & \square \\ \hline \end{array} \quad (\text{B26})$$

for spin-0 and spin-1 baryons, respectively. We again specify the $|S = 0, S_z = 0\rangle$ spin state, for which the only spin configuration is the well-known anti-symmetric two-body spin-singlet state. The flavor configurations with $Q = 0$ are

$$\left| -\frac{3}{2} \quad +\frac{3}{2} \right\rangle, \quad \left| +\frac{3}{2} \quad -\frac{3}{2} \right\rangle, \quad \left| -\frac{1}{2} \quad +\frac{1}{2} \right\rangle, \quad \left| +\frac{1}{2} \quad -\frac{1}{2} \right\rangle. \quad (\text{B27})$$

When paired with the allowed spin configuration and symmetrized, these generate the baryon spin-flavor eigenstates

$$|\mathbf{B}_1^0\rangle = \frac{1}{2} \left(\left| -\frac{3}{2} \quad +\frac{3}{2} \right\rangle - \left| +\frac{3}{2} \quad -\frac{3}{2} \right\rangle \right) \otimes (|\uparrow\downarrow\rangle - |\downarrow\uparrow\rangle), \quad (\text{B28})$$

$$|\mathbf{B}_2^0\rangle = \frac{1}{2} \left(\left| -\frac{1}{2} \quad +\frac{1}{2} \right\rangle - \left| +\frac{1}{2} \quad -\frac{1}{2} \right\rangle \right) \otimes (|\uparrow\downarrow\rangle - |\downarrow\uparrow\rangle), \quad (\text{B29})$$

which, when written in the basis that diagonalizes J^2 and acted on with J_\pm , provide the $\text{SU}(2)_L$ singlet

$$|\mathbf{J}_0^0\rangle = \frac{1}{\sqrt{2}} (|\mathbf{B}_1^0\rangle - |\mathbf{B}_2^0\rangle) \quad (\text{B30})$$

and 5-plet

$$\begin{pmatrix} |\mathbf{J}_2^{++}\rangle \\ |\mathbf{J}_2^+\rangle \\ |\mathbf{J}_2^0\rangle \\ |\mathbf{J}_2^-\rangle \\ |\mathbf{J}_2^{--}\rangle \end{pmatrix} = \begin{pmatrix} |\mathbf{B}^{++}\rangle \\ |\mathbf{B}^+\rangle \\ \frac{1}{\sqrt{2}} (|\mathbf{B}_1^0\rangle + |\mathbf{B}_2^0\rangle) \\ |\mathbf{B}^-\rangle \\ |\mathbf{B}^{--}\rangle \end{pmatrix}, \quad (\text{B31})$$

where

$$|\mathbf{B}^{++}\rangle = \frac{1}{2} \left(\left| +\frac{1}{2} \quad +\frac{3}{2} \right\rangle - \left| +\frac{3}{2} \quad +\frac{1}{2} \right\rangle \right) \otimes (|\uparrow\downarrow\rangle - |\downarrow\uparrow\rangle) \quad (\text{B32})$$

$$|\mathbf{B}^+\rangle = \frac{1}{2} \left(\left| -\frac{1}{2} \quad +\frac{3}{2} \right\rangle - \left| +\frac{3}{2} \quad -\frac{1}{2} \right\rangle \right) \otimes (|\uparrow\downarrow\rangle - |\downarrow\uparrow\rangle), \quad (\text{B33})$$

and so on for the negatively-charged states. These multiplets indicate the decomposition

$$\text{SU}(4) \supset \text{SU}(2)_L \quad (\text{B34})$$

$$\begin{array}{|c|} \hline \square \\ \hline \square \\ \hline \end{array} \rightarrow \mathbf{5} \oplus \mathbf{1},$$

for our embedding of $SU(2)_L$ in flavor $SU(4)$. The only reason why we chose both benchmark models to have the same $SU(2)_L$ multiplets is because the singlet and 5-plet combination is the simplest case where there is a singlet in the spectrum and mixing of neutral states in different representations.

In the electroweak-symmetric phase of the SM, gauge invariance guarantees that each 5-plet baryon state in Eq. (B22) is a mass eigenstate with exactly the same mass, and likewise for the states in Eq. (B31). Then, the singlets in Eqs. (B21) and (B30) are mass eigenstates with different masses. In the electroweak-broken phase, charge differences cause the masses of states in the 5-plets to split apart, and the neutral $SU(2)_L$ eigenstates will no longer be mass eigenstates. App. C details the mass calculation and implications of these observations.

3. More Insights on the $SU(N_f) \rightarrow SU(2)_L$ Decomposition

There is more than one way to construct baryon wavefunctions and determine the decomposition of the flavor representation into representations of $SU(2)_L$. The algorithm we described in App. B2 is simple to perform, naturally combines flavor states and spin states, and is independent of our foreknowledge of the flavor representation. The fact that the number of baryons obtained by that algorithm agrees with the dimension of the representation in Eq. (B2) is thus a valuable consistency check. However, as N_c and N_f become larger, the brute-force symmetrization of states becomes computationally slow (particularly when $N_c \gtrsim 6$). We therefore devised an alternative algorithm to perform the $SU(N_f) \rightarrow SU(2)_L$ decomposition by leveraging the symmetry structure of the tableau in Eq. (B2).

Our alternative algorithm begins by finding all flavor states with the middlest charge in the same way as described in App. B2. Then, one applies *Young symmetrizers* (see e.g. [129]) to each flavor state.¹⁰ Consider labeling each box in the tableau in Eq. (B2) with a number corresponding to each particle. For particle labels in each column of the tableau, one anti-symmetrizes the states over that subset of particles (adding up all permutations of the subset of particles weighted by the parity of the permutation). Then, for particle labels in each row of the tableau, one symmetrizes the states over that subset of particles.¹¹ Take for example the tableau in Eq. (B5) for spin-0 baryons with $(N_c, N_f) = (4, 3)$. One can label the boxes as¹²

$$\begin{array}{|c|c|} \hline 1 & 2 \\ \hline 3 & 4 \\ \hline \end{array} \quad (\text{B35})$$

Then, take the flavor state $|f\rangle = |-00+\rangle$ as an example. One anti-symmetrizes over particles (1, 3) and (2, 4)

$$|f\rangle \xrightarrow{[13]} |f_{[13]}\rangle = |-00+\rangle - |00-\rangle \quad (\text{B36})$$

$$|f_{[13]}\rangle \xrightarrow{[24]} |f_{[13][24]}\rangle = |-00+\rangle - |00-\rangle - |-+00\rangle + |0+-0\rangle, \quad (\text{B37})$$

then symmetrizes over (1, 2) and (3, 4)

$$|f_{[13][24]}\rangle \xrightarrow{(12)} |f_{[13][24](12)}\rangle = |-00+\rangle - 2|00-\rangle - |-+00\rangle + |0+-0\rangle \quad (\text{B38})$$

$$+ |0-0+\rangle - |+ -00\rangle + |+0-0\rangle \quad (\text{B39})$$

$$|f_{[13][24](12)}\rangle \xrightarrow{(34)} |f_{[13][24](12)(34)}\rangle = |-00+\rangle - 2|00-\rangle - 2|-+00\rangle + |0+-0\rangle \quad (\text{B40})$$

$$+ |0-0+\rangle - 2|+-00\rangle + |+0-0\rangle + |-0+0\rangle \quad (\text{B41})$$

$$- 2|00+-\rangle + |0+0-\rangle + |0-+0\rangle + |+00-\rangle. \quad (\text{B42})$$

Doing this procedure for each middlest-charge flavor state and using the Gram-Schmidt process to eliminate the redundancy of the resulting set of states yields a complete, orthogonal basis of flavor states in the desired flavor representation with the desired charge. One can then diagonalize J^2 as above to determine the $SU(2)_L$ representations.

¹⁰ One typically applies Young symmetrizers to tensors. We are applying them to components of a tensor.

¹¹ The choice to anti-symmetrize first and symmetrize second is arbitrary.

¹² The numbering scheme is arbitrary as one performs the procedure for all relevant permutations.

This alternative version of the algorithm makes no reference to spin states, though it could be extended to construct the full spin-flavor wavefunctions.

One can interpret each symmetrizer as a linear operator. Then, the product of symmetrizers corresponding to a Young tableau is itself an operator, which one can call the “tableau operator”. If the symmetries of a particular state are incompatible with the symmetries of the desired flavor representation (*e.g.* a totally symmetric state when the representation is not totally symmetric), then the tableau operator maps that state to the null state. In other words, the vector space of states whose symmetries are incompatible with the desired representation is the kernel of the tableau operator. By consequence, the dimension of the vector space of states that do have compatible symmetries equals the rank (*i.e.* the number of linearly independent rows of the matrix) of the tableau operator. Since we are only considering the action of the tableau operator on the space of states with the middle charge, and each $SU(2)_L$ multiplet contains exactly one such state, the rank of the tableau operator equals the number of $SU(2)_L$ multiplets in the decomposition.¹³

With the speed of the Young symmetrizer algorithm, we can easily compute the $SU(N_f) \rightarrow SU(2)_L$ decompositions for the larger $N_{c,f}$ shown in Table B1. As discussed in App. A, Landau poles quickly appear for the larger representations, so one can consider most of the table a group theory exercise rather than a statement about phenomenology. We observe several interesting patterns in the decompositions, which we describe without proof that they hold for all $N_{c,f}$:

1. For $N_c = 2$, the spin-1 representations for a particular N_f become the spin-0 representations for $N_f + 1$.
2. For N_c even and not divisible by 4, the smallest spin-0 representation is a singlet for N_f even and a triplet for N_f odd. For spin-1, this is reversed.
3. For N_c divisible by 4, the smallest spin-0 representation is a singlet, and the smallest spin-1 representation is a triplet.
4. For $N_c = 3$, we have found no instances of spin-1/2 singlets. There are, however, instances of spin-3/2 singlets for $N_c = 3$ and spin-1/2 singlets for larger odd N_c .
5. When holding N_c fixed and increasing N_f by 1, the size of the largest representation increases by N_c .

We invite the reader to attempt to prove these patterns or observe others.

¹³ Another (less efficient) way to find the $SU(2)_L$ decomposition would be to compute the ranks of the tableau operators that act on states with each possible charge. The differences between these ranks indicates the differences in the number of states in the desired flavor representation with each charge, from which one can deduce the number of multiplets with a particular maximum charge. For example, if there are n states with $Q = 1$ and $n + 2$ states with $Q = 0$, then there are two singlets in the spectrum. This way, one can perform the $SU(2)_L$ decomposition without ever diagonalizing J^2 .

(N_c, N_f)	Lowest-Spin Baryon $SU(2)_L$ Representations	Next-to-Lowest-Spin Baryon $SU(2)_L$ Representations
(2,2)	1	3
(2,3)	3	5 ⊕ 1
(2,4)	5 ⊕ 1	7 ⊕ 3
(2,5)	7 ⊕ 3	9 ⊕ 5 ⊕ 1
(2,6)	9 ⊕ 5 ⊕ 1	11 ⊕ 7 ⊕ 3
(3,2)	2	4
(3,3)	5 ⊕ 3	7 ⊕ 3
(3,4)	8 ⊕ 6 ⊕ 4 ⊕ 2	10 ⊕ 6 ⊕ 4
(3,5)	11 ⊕ 9 ⊕ 7 ⊕ 5 ⊕ 3	13 ⊕ 9 ⊕ 7 ⊕ 5 ⊕ 1
(3,6)	14 ⊕ 12 ⊕ 10 ⊕ 8 ⊕ 6 ⊕ 4 ⊕ 2	16 ⊕ 12 ⊕ 10 ⊕ 8 ⊕ 6 ⊕ 4
(4,2)	1	3
(4,3)	5 ⊕ 1	7 ⊕ 5 ⊕ 3
(4,4)	9 ⊕ 5 ⊕ 5 ⊕ 1	11 ⊕ 9 ⊕ 7 ⊕ 7 ⊕ 5 ⊕ 3 ⊕ 3
(4,5)	13 ⊕ 9 ⊕ 9 ⊕ 7 ⊕ 5 ⊕ 5 ⊕ 1 ⊕ 1	15 ⊕ 13 ⊕ 11 ⊕ 11 ⊕ 9 ⊕ 9 ⊕ 7 ⊕ 7 ⊕ 7 ⊕ 5 ⊕ 5 ⊕ 3 ⊕ 3
(4,6)	17 ⊕ 13 ⊕ 13 ⊕ 11 ⊕ 9 ⊕ 9 ⊕ 9 ⊕ 7 ⊕ 5 ⊕ 5 ⊕ 5 ⊕ 1 ⊕ 1	19 ⊕ 17 ⊕ 15 ⊕ 15 ⊕ 13 ⊕ 13 ⊕ 11 ⊕ 11 ⊕ 11 ⊕ 11 ⊕ 9 ⊕ 9 ⊕ 9 ⊕ 7 ⊕ 7 ⊕ 7 ⊕ 7 ⊕ 5 ⊕ 5 ⊕ 3 ⊕ 3 ⊕ 3
(5,2)	2	4
(5,3)	7 ⊕ 5 ⊕ 3	9 ⊕ 7 ⊕ 5 ⊕ 3
(5,4)	12 ⊕ 10 ⊕ 8 ⊕ 8 ⊕ 6 ⊕ 6 ⊕ 4 ⊕ 4 ⊕ 2	14 ⊕ 12 ⊕ 10 ⊕ 10 ⊕ 8 ⊕ 8 ⊕ 6 ⊕ 6 ⊕ 4 ⊕ 4 ⊕ 2
(5,5)	17 ⊕ 15 ⊕ 13 ⊕ 13 ⊕ 11 ⊕ 11 ⊕ 11 ⊕ 9 ⊕ 9 ⊕ 9 ⊕ 9 ⊕ 7 ⊕ 7 ⊕ 7 ⊕ 5 ⊕ 5 ⊕ 5 ⊕ 5 ⊕ 3 ⊕ 3 ⊕ 1	19 ⊕ 17 ⊕ 15 ⊕ 15 ⊕ 13 ⊕ 13 ⊕ 13 ⊕ 11 ⊕ 11 ⊕ 11 ⊕ 9 ⊕ 9 ⊕ 9 ⊕ 9 ⊕ 7 ⊕ 7 ⊕ 7 ⊕ 7 ⊕ 5 ⊕ 5 ⊕ 5 ⊕ 3 ⊕ 3 ⊕ 1
(6,2)	1	3
(6,3)	7 ⊕ 3	9 ⊕ 7 ⊕ 5 ⊕ 5 ⊕ 1
(6,4)	13 ⊕ 9 ⊕ 9 ⊕ 7 ⊕ 5 ⊕ 5 ⊕ 1 ⊕ 1	15 ⊕ 13 ⊕ 11 ⊕ 11 ⊕ 11 ⊕ 9 ⊕ 9 ⊕ 7 ⊕ 7 ⊕ 7 ⊕ 7 ⊕ 5 ⊕ 5 ⊕ 3 ⊕ 3 ⊕ 3
(6,5)	19 ⊕ 15 ⊕ 15 ⊕ 13 ⊕ 13 ⊕ 11 ⊕ 11 ⊕ 11 ⊕ 9 ⊕ 9 ⊕ 7 ⊕ 7 ⊕ 7 ⊕ 7 ⊕ 7 ⊕ 5 ⊕ 3 ⊕ 3 ⊕ 3	21 ⊕ 19 ⊕ 17 ⊕ 17 ⊕ 17 ⊕ 15 ⊕ 15 ⊕ 15 ⊕ 13 ⊕ 13 ⊕ 13 ⊕ 13 ⊕ 13 ⊕ 13 ⊕ 11 ⊕ 11 ⊕ 11 ⊕ 11 ⊕ 11 ⊕ 9 ⊕ 9 ⊕ 9 ⊕ 9 ⊕ 9 ⊕ 9 ⊕ 9 ⊕ 9 ⊕ 7 ⊕ 7 ⊕ 7 ⊕ 7 ⊕ 7 ⊕ 5 ⊕ 5 ⊕ 5 ⊕ 5 ⊕ 5 ⊕ 5 ⊕ 5 ⊕ 3 ⊕ 3 ⊕ 1 ⊕ 1 ⊕ 1
(7,2)	2	4
(7,3)	9 ⊕ 7 ⊕ 5 ⊕ 3	11 ⊕ 9 ⊕ 7 ⊕ 7 ⊕ 5 ⊕ 3
(7,4)	16 ⊕ 14 ⊕ 12 ⊕ 12 ⊕ 10 ⊕ 10 ⊕ 10 ⊕ 8 ⊕ 8 ⊕ 8 ⊕ 6 ⊕ 6 ⊕ 6 ⊕ 4 ⊕ 4 ⊕ 4 ⊕ 2	18 ⊕ 16 ⊕ 14 ⊕ 14 ⊕ 14 ⊕ 12 ⊕ 12 ⊕ 12 ⊕ 10 ⊕ 10 ⊕ 10 ⊕ 10 ⊕ 8 ⊕ 8 ⊕ 8 ⊕ 8 ⊕ 6 ⊕ 6 ⊕ 6 ⊕ 6 ⊕ 4 ⊕ 4 ⊕ 4 ⊕ 2 ⊕ 2
(8,2)	1	3
(8,3)	9 ⊕ 5 ⊕ 1	11 ⊕ 9 ⊕ 7 ⊕ 7 ⊕ 5 ⊕ 3
(8,4)	17 ⊕ 13 ⊕ 13 ⊕ 11 ⊕ 9 ⊕ 9 ⊕ 9 ⊕ 7 ⊕ 5 ⊕ 5 ⊕ 5 ⊕ 1 ⊕ 1	19 ⊕ 17 ⊕ 15 ⊕ 15 ⊕ 15 ⊕ 13 ⊕ 13 ⊕ 13 ⊕ 11 ⊕ 11 ⊕ 11 ⊕ 11 ⊕ 11 ⊕ 9 ⊕ 9 ⊕ 9 ⊕ 9 ⊕ 7 ⊕ 7 ⊕ 7 ⊕ 7 ⊕ 7 ⊕ 7 ⊕ 5 ⊕ 5 ⊕ 5 ⊕ 3 ⊕ 3 ⊕ 3 ⊕ 3

TABLE B1: Decomposition of the flavor representation in Eq. (B2) into representations of its gauged $SU(2)_L$ subgroup for many $N_{c,f}$ combinations. The lowest-spin baryons are spin-0 for N_c even and spin-1/2 for N_c odd. The next-to-lowest-spin baryons are spin-1 for N_c even and spin-3/2 for N_c odd.

4. Scalar Quarks

We have so far considered only spin-1/2 dark quarks, but scalar quarks also have interesting phenomenology. The dark sector Lagrangian would be modified to include the scalar's quartic self-interactions and dimension-4 couplings between the scalar and the SM Higgs boson. The Higgs coupling induces a direct detection signal due to Higgs boson exchange. When the scalar is heavy and integrated out, the Higgs coupling also induces (at one loop) a dimension-6 effective interaction between the Higgs (including its Goldstones) and dark gluons, which facilitates production and decay of dark sector glueballs in a collider context [23, 25, 39]. One could still use the quark model in the heavy quark limit, but the inter-quark potential would include terms due to Higgs boson exchange and the quartic coupling in addition to vector boson exchange.

We can use similar arguments as above to characterize baryon states and their representations. With their bosonic constituents, baryon composites of scalar quarks have totally symmetric wavefunctions. The color wavefunction is still anti-symmetric, and the spins are trivial, so the combination of flavor and spatial wavefunctions must be totally anti-symmetric. Suppose the spatial wavefunction is totally symmetric. Then, the only allowed flavor representation is

$$\begin{aligned}
 & N_c \left\{ \begin{array}{c} \square \\ \vdots \\ \square \end{array} \right. \tag{B43} \\
 & \text{dimension} = \frac{N_f!}{N_c!(N_f - N_c)!},
 \end{aligned}$$

since it must be totally anti-symmetric.

However, this representation of $SU(N_f)$ does not exist if $N_c > N_f$, as a Young tableau for $SU(N_f)$ cannot have a column with more than N_f boxes. In such cases, baryons with symmetric spatial wavefunctions are *forbidden*, and the lowest-lying states are p -wave. With an anti-symmetric spatial wavefunction, the only allowed flavor representation is

$$\begin{aligned}
 & \underbrace{\square \cdots \square}_{\tilde{N}_c} \tag{B44} \\
 & \text{dimension} = \frac{(N_f - 1 + N_c)!}{N_c!(N_f - 1)!}.
 \end{aligned}$$

These representations can be decomposed into representations of $SU(2)_L$, as shown in Table B2. Note in particular that if $N_c = N_f$, the representation in Eq. (B43) is the trivial representation of $SU(N_f)$, so the only possible $SU(2)_L$ multiplet is the singlet. The version of our algorithm with Young symmetrizers naturally performs the decomposition for baryons with scalar constituents. For the $SU(N_f)$ representations we have decomposed, singlets appear slightly less often compared to the case of spin-1/2 constituents.

We can sort each spectrum of multiplets into categories analogous to those defined in Sec. II B:

- I. There is only a singlet ($N_c = N_f$).
- II. There is a singlet accompanied by larger odd representations.
- III. There are no singlets, but there are neutral states.
- IV. There are no neutral states.

Note that the decomposition of the flavor representation into representations of $SU(2)_L$ for $N_c = 2$ is the same for lowest-lying baryons with scalar constituents and spin-0 baryons with spin-1/2 constituents because in this case, the representations in Eq. (B2) and Eq. (B43) are equivalent.

(N_c, N_f)	Baryon $SU(2)_L$ Representations (Scalar Constituents)	Category
(2,2)	1	I
(2,3)	3	III
(2,4)	5 \oplus 1	II
(2,5)	7 \oplus 3	III
(2,6)	9 \oplus 5 \oplus 1	II
(3,2)	4	IV
(3,3)	1	I
(3,4)	4	IV
(3,5)	7 \oplus 3	III
(3,6)	10 \oplus 6 \oplus 4	IV
(4,2)	5	III
(4,3)	9 \oplus 5 \oplus 1	II
(4,4)	1	I
(4,5)	5	III
(4,6)	9 \oplus 5 \oplus 1	II
(5,2)	6	IV
(5,3)	11 \oplus 7 \oplus 3	III
(5,4)	16 \oplus 12 \oplus 10 \oplus 8 \oplus 6 \oplus 4	IV
(5,5)	1	I
(5,6)	6	IV
(6,2)	7	III
(6,3)	13 \oplus 9 \oplus 5 \oplus 1	II
(6,4)	19 \oplus 15 \oplus 13 \oplus 11 \oplus 9 \oplus 7 \oplus 7 \oplus 3	III
(6,5)	25 \oplus 21 \oplus 19 \oplus 17 \oplus 17 \oplus 15 \oplus 13 \oplus 13 \oplus 13 \oplus 11 \oplus 9 \oplus 9 \oplus 9 \oplus 7 \oplus 5 \oplus 5 \oplus 1 \oplus 1	II
(6,6)	1	I
(7,2)	8	IV
(7,3)	15 \oplus 11 \oplus 7 \oplus 3	III
(7,4)	22 \oplus 18 \oplus 16 \oplus 14 \oplus 12 \oplus 10 \oplus 10 \oplus 8 \oplus 6 \oplus 4	IV
(8,2)	9	III
(8,3)	17 \oplus 13 \oplus 9 \oplus 5 \oplus 1	II
(8,4)	25 \oplus 21 \oplus 19 \oplus 17 \oplus 15 \oplus 13 \oplus 13 \oplus 11 \oplus 9 \oplus 9 \oplus 7 \oplus 5 \oplus 1	II

TABLE B2: Decomposition of the flavor representation in Eq. (B43) (for $N_c \leq N_f$) or Eq. (B44) (for $N_c > N_f$) for baryons with scalar constituents, as in Table B1. We also indicate the category of each spectrum of multiplets defined in App. B4.

Appendix C: Further Details on the Mass Calculation

In the limit where the dark quark mass m_q is significantly larger than the dark sector confinement scale Λ_χ , mesons and baryons are well-approximated as weakly-coupled bound states of non-relativistic constituents. In Ref. [61], this quark model picture is applied to the SM, where the physical quark masses are less than the confinement scale, and non-perturbative effects give large contributions to hadron masses. Nonetheless, this approach predicts SM hadron mass splittings fairly well using non-perturbative dressed quark masses. In the heavy quark limit of our model, we treat non-perturbative and relativistic effects as negligible, so we expect the quark model prediction to be a valid approximation of hadron masses (not only their splittings) using physical quark masses. We cannot reliably compute the hadron masses when m_q is not significantly greater than Λ_χ , but our qualitative conclusions concerning relative mass splittings and mixings likely still hold as these are driven by perturbative electroweak effects.

1. The Mass Hamiltonian

The mass operator in Eq. (3) comes from the Hamiltonian

$$H = H_{\text{free}} + \sum_{i < j} V_{ij}, \quad (\text{C1})$$

where V_{ij} is the inter-quark potential, and H_{free} is the free Hamiltonian

$$H_{\text{free}} = \sum_i \left(m_i + \frac{p_i^2}{2m_i} \right), \quad (\text{C2})$$

in the non-relativistic approximation. At first order in the gauge couplings, the inter-quark potential comes from exchange of a single gauge boson. For massless gauge bosons (*i.e.* the photon and dark gluons) and at first order in the non-relativistic expansion in p^2/m_q^2 , this potential is the Fermi-Breit potential familiar from the Hydrogen atom in non-relativistic quantum mechanics.

In addition to the dark sector coupling, the dark gluon potential in Eq. (3) includes a color factor $-(N_c + 1)/(2N_c)$ from contractions of $SU(N_c)$ generators in the fundamental representation with anti-symmetric baryon color wavefunctions. For mesons, this factor should be replaced with $-(N_c^2 - 1)/(2N_c)$, where the sign is from fermion statistics, and the N_c -dependence is from contracting $SU(N_c)$ generators with color-singlet wavefunctions. In the SM with $N_c = 3$, these color factors reproduce the $-2/3$ for baryons and $-4/3$ for mesons found in Ref. [61].

In the electroweak-symmetric limit, the photon and Z contributions in Eq. (3) sum to the contribution of the third $SU(2)_L$ gauge boson, the W^3 , since $\alpha_{\text{EM}} + \alpha_W \cos^2 \theta_W = \alpha_W$. The raising and lowering operators in Eq. (3) allow the W boson to mix hadron states with different flavor content, which is why the spin-flavor eigenstates described in App. B are not in general equivalent to $SU(2)_L$ eigenstates or mass eigenstates. In the $m_q, \Lambda_\chi \gg m_W$ limit, electroweak symmetry breaking is “small” in the dark sector, and mass eigenstates should be nearly identical to $SU(2)_L$ eigenstates as shown in Fig. 1. In the $m_q, \Lambda_\chi \ll m_W$ limit where one can integrate out the W , spin-flavor eigenstates should be nearly identical to mass eigenstates as their mixing due to the W is suppressed. We indeed see this behavior in Fig. 1, as the overlaps of the mass eigenstates with the $SU(2)_L$ eigenstates approach the overlaps of the spin-flavor eigenstates with the $SU(2)_L$ eigenstates as m_q becomes small.

In order to incorporate finite-mass effects of the W and Z , we require a generalization of the Fermi-Breit potential whose 0th order term in the non-relativistic expansion is the Yukawa potential rather than the Coulomb potential. Ref. [64] derived that, up to color factors and couplings, the inter-quark potential is

$$V_{ij} = V_0(r) \quad (\text{C3})$$

$$+ \left(\frac{1}{8m_i^2} + \frac{1}{8m_j^2} \right) \nabla^2 V_0(r) \quad (\text{C4})$$

$$+ \left[\left(\frac{1}{2m_i^2} + \frac{1}{m_i m_j} \right) \mathbf{S}_i + \left(\frac{1}{2m_j^2} + \frac{1}{m_i m_j} \right) \mathbf{S}_j \right] \cdot \boldsymbol{\ell} \frac{V_0'(r)}{r} \quad (\text{C5})$$

$$+ \frac{1}{m_i m_j} \left[\frac{2}{3} \mathbf{S}_i \cdot \mathbf{S}_j \nabla^2 V_0(r) \right] \quad (\text{C6})$$

$$+ \left((\mathbf{S}_i \cdot \hat{r})(\mathbf{S}_j \cdot \hat{r}) - \frac{1}{3} \mathbf{S}_i \cdot \mathbf{S}_j \right) \left(V_0''(r) - \frac{V_0'(r)}{r} \right) \quad (\text{C7})$$

$$- \frac{1}{8m_i m_j} (\mathbf{p}_i \cdot \mathbf{p}_j, V_0(r)) + 2p_i^\alpha V_0(r) p_j^\alpha \quad (\text{C8})$$

$$- \frac{1}{4m_i m_j} \left(\left\{ p_i^\alpha p_j^\beta, \hat{r}^\alpha \hat{r}^\beta W(r) \right\} + 2p_i^\alpha \hat{r}^\alpha \hat{r}^\beta W(r) p_j^\beta \right) \quad (\text{C9})$$

at $\mathcal{O}(p^2/m^2)$, where $V_0(r)$ is the potential at 0th order in the non-relativistic expansion, $W(r) = -rV_0'(r)/2$, ℓ is the angular momentum operator, \hat{r} is the unit vector in the direction of the inter-quark separation $\mathbf{r} = \mathbf{r}_i - \mathbf{r}_j$, and α, β are Cartesian indices.¹⁴ One may recognize Eqs. (C4) and (C5) as the fine-structure correction and Eqs. (C6) and (C7) as the hyperfine-structure correction.

For hadrons with symmetric spatial wavefunctions, the spin-orbit coupling in Eq. (C5) and tensor force contribution in Eq. (C7) do not contribute, since ℓ has odd parity and $\langle (\hat{r} \cdot \mathbf{S}_i)(\hat{r} \cdot \mathbf{S}_j) \rangle \rightarrow \langle \mathbf{S}_i \cdot \mathbf{S}_j \rangle / 3$ [132]. The remaining contributions are $V_0(r)$, the Darwin term in Eq. (C4), the spin-spin coupling in Eq. (C6), and the orbit-orbit coupling in Eqs. (C8) and (C9). Using $V_0(r) = e^{-m_V r}/r$ for the Yukawa potential, expanding out the momentum operators in terms of gradients, taking the expectation value with respect to a symmetric spatial wavefunction, setting $m_{i,j} = m_q$, and re-inserting coupling coefficients, one recovers Eq. (3).

The contact terms that arise from the spin-spin coupling and Darwin terms are not suppressed by the mass of the exchanged boson. It is unclear how important the contact terms from W and Z exchange are to the quark model calculation in the SM, which has additional complications of chiral couplings (which Eq. (C3) does not accommodate) and non-trivial relativistic and non-perturbative corrections. In our model, these contact terms are indispensable for correctly predicting which baryons species is lightest, particularly when $m_W \ll m_q$.

2. Quark Mass Splittings

Invariance of the Lagrangian under $SU(2)_L$ requires that the tree-level quark masses in our model must be degenerate. Spontaneous breaking of electroweak symmetry breaks that degeneracy at one loop due to self-energy corrections. These have the form



$$\text{Q} \rightarrow \text{Q} \quad (\text{C10})$$

where the boson in the loop can be a photon, dark gluon, W , or Z . In the mass Hamiltonian, we work to leading order in the gauge couplings, so corrections to m_q in the inter-quark potential are higher-order. In the free Hamiltonian, however, the one-loop correction to m_q is at the same order in perturbation theory as the inter-quark potential. We therefore use

$$m_i = m_q - \Sigma_i^{1\text{-loop}}(m_q) + \mathcal{O}(\alpha^2), \quad (\text{C11})$$

where $\Sigma_i^{1\text{-loop}}(m_q)$ is the one-loop self-energy of the i^{th} quark evaluated at $\not{p} = m_q$, and $\mathcal{O}(\alpha^2)$ represents corrections at higher order in the gauge couplings [133]. Then, the free Hamiltonian has the form

$$H_{\text{free}} = \sum_i \left(m_q + \frac{p_i^2}{2m_q} + \left(\frac{p_i^2}{2m_q^2} - 1 \right) \Sigma_i^{1\text{-loop}}(m_q) \right) + \mathcal{O}(\alpha^2). \quad (\text{C12})$$

This correction can cause our predictions for baryon masses to be greater than $N_c m_q$, even when the expectation value of the inter-quark potential is negative.

¹⁴ In standard derivations of the Fermi-Breit potential (*e.g.* Refs. [130, 131]), the ordering of position and momentum operators is not handled carefully, so applying the same calculations to massive boson exchange does not ensure a Hermitian potential. When transforming the potential from momentum space to position space, one must keep initial and final momentum operators written on opposite sides of position operators so that p_{initial} acts on $|p_{\text{initial}}\rangle$ and p_{final} acts on $\langle p_{\text{final}}|$.

The self-energy is given by

$$\begin{aligned} \Sigma_i^{1\text{-loop}}(m_q) = & -\frac{m_q}{2\pi} \left[\left(\alpha_{\text{EM}} Q_i^2 + \frac{N_c^2 - 1}{2N_c} \alpha_\chi \right) f(0) + \alpha_W \cos^2(\theta_W) Q_i^2 f(m_Z/m_q) \right. \\ & \left. + \alpha_W \left(\frac{N_f^2 - 1}{4} - Q_i^2 \right) f(m_W/m_q) \right], \end{aligned} \quad (\text{C13})$$

where

$$f(r) = \frac{1}{2} \left(4 + 3 \ln \left(\frac{\mu^2}{m_q^2} \right) - r^4 \ln r + r^2 - \frac{r}{2} \sqrt{r^2 - 4} (r^2 + 2) \ln \left(\frac{r^2 - 2 - r\sqrt{r^2 - 4}}{2} \right) \right), \quad (\text{C14})$$

with μ the renormalization scale, using Feynman gauge and the $\overline{\text{MS}}$ scheme.¹⁵ We define the tree-level mass to equal m_q at the scale m_q and therefore evaluate the self-energy and running couplings therein at $\mu = m_q$. One should interpret the Q_i^2 factors as operators acting on spin-flavor wavefunctions. Note that in the electroweak-symmetric limit, the terms in Eq. (C13) with Q_i^2 cancel, and the remaining $(N_f^2 - 1)/4$ prefactor on the electroweak contribution is the Casimir invariant C_2 defined by $J_{ik}^a J_{kj}^a = C_2 \delta_{ij}$ for the N_f -dimensional representation of $\text{SU}(2)_L$. This factor is the $\text{SU}(2)_L$ analog of the $(N_c^2 - 1)/(2N_c)$ color factor that appears in the dark gluon contribution [134].

So far, our discussion of the mass calculation has been in the effective field theory of quarks rather than the effective field theory of hadrons. In the theory of hadrons, mass splittings derive from diagrams of the same form as Eq. (C10) with the quark line replaced by hadron and the gauge boson a photon, W , or Z . In the limit where W and Z cannot resolve the structure of the hadron, *i.e.* when $1/m_{W,Z}$ is much greater than the hadron's characteristic size scale, we expect the quark model calculation of hadron mass splittings to approximately match onto the mass splittings computed in the effective field theory of hadrons. As computed in Ref. [65], for vector-like fermions or scalars much heavier than $m_{W,Z}$ with zero hypercharge in some multiplet of $\text{SU}(2)_L$, the mass splitting between the $Q = 1$ and $Q = 0$ components of the multiplet is

$$M_{Q=1} - M_{Q=0} \simeq \alpha_W m_W \sin(\theta_W/2) \simeq 166 \text{ MeV}. \quad (\text{C15})$$

In the limit $m_q, \Lambda_\chi \gg m_W$, our prediction for the splitting between singly-charged and neutral hadrons in the same $\text{SU}(2)_L$ multiplet approximately reproduces this result. This serves as a check on our calculation.

3. Spin-flavor Matrix Elements

The charge, spin, and ladder operators in Eq. (3) act on the spin-flavor wavefunctions found in App. B 2. Here, we discuss the actions of these operators on $\text{SU}(2)_L$ eigenstates in the $(N_c, N_f) = (4, 3)$ and $(2, 4)$ models. We use the following notation for these spin-flavor operators as matrices acting on baryon states:

$$\langle \mathcal{J}^0 | Q_i Q_j | \mathcal{J}^0 \rangle \equiv \begin{pmatrix} \langle \mathcal{J}_0^0 | \\ \langle \mathcal{J}_2^0 | \end{pmatrix} \left(\sum_{i < j} Q_i Q_j \right) \begin{pmatrix} | \mathcal{J}_0^0 \rangle \\ | \mathcal{J}_2^0 \rangle \end{pmatrix}, \quad (\text{C16})$$

and so on for other operators and $\text{SU}(2)_L$ eigenstates. We abbreviate $(J_+^i J_-^j + J_-^i J_+^j)/2$ as $J_\pm^i J_\mp^j$. As discussed in App. C 2, we will need the $\sum_i Q_i^2$ operator in addition to the operators appearing in the inter-quark potential. When acting on hadron states that are not spin-flavor eigenstates, the operators $Q_i Q_j$, $Q_i Q_j \mathbf{S}_i \cdot \mathbf{S}_j$, and Q_i^2 have off-diagonal matrix elements.

In the $(4, 3)$ model, the required matrix elements are

¹⁵ For the loops with massless gauge bosons, an apparent infrared divergence can be regulated by introducing a gauge boson mass and taking the limit of that mass going to zero. Despite the logarithms, $f(r)$ has a well-defined $r \rightarrow 0^+$ limit.

$$\langle \mathcal{J}^0 | Q_i Q_j | \mathcal{J}^0 \rangle = \begin{pmatrix} -4/3 & \sqrt{2}/3 \\ \sqrt{2}/3 & -5/3 \end{pmatrix} \quad \langle \mathcal{J}^0 | Q_i Q_j \mathbf{S}_i \cdot \mathbf{S}_j | \mathcal{J}^0 \rangle = \begin{pmatrix} 2/3 & -11/\sqrt{72} \\ -11/\sqrt{72} & 19/12 \end{pmatrix} \quad (\text{C17})$$

$$\langle \mathcal{J}^0 | J_\pm^i J_\mp^j | \mathcal{J}^0 \rangle = \begin{pmatrix} -8/3 & -\sqrt{2}/3 \\ -\sqrt{2}/3 & 2/3 \end{pmatrix} \quad \langle \mathcal{J}^0 | J_\pm^i J_\mp^j \mathbf{S}_i \cdot \mathbf{S}_j | \mathcal{J}^0 \rangle = \begin{pmatrix} 4/3 & 11/\sqrt{72} \\ 11/\sqrt{72} & 7/6 \end{pmatrix} \quad (\text{C18})$$

$$\langle \mathcal{J}^0 | Q_i^2 | \mathcal{J}^0 \rangle = \begin{pmatrix} 8/3 & -\sqrt{8}/3 \\ -\sqrt{8}/3 & 10/3 \end{pmatrix} \quad \langle \mathcal{J}^0 | \mathbf{S}_i \cdot \mathbf{S}_j | \mathcal{J}^0 \rangle = \begin{pmatrix} -3/2 & 0 \\ 0 & -3/2 \end{pmatrix} \quad (\text{C19})$$

$$\langle \mathcal{J}^+ | Q_i Q_j | \mathcal{J}^+ \rangle = -1 \quad \langle \mathcal{J}^+ | Q_i Q_j \mathbf{S}_i \cdot \mathbf{S}_j | \mathcal{J}^+ \rangle = 5/4 \quad (\text{C20})$$

$$\langle \mathcal{J}^+ | J_\pm^i J_\mp^j | \mathcal{J}^+ \rangle = 0 \quad \langle \mathcal{J}^+ | J_\pm^i J_\mp^j \mathbf{S}_i \cdot \mathbf{S}_j | \mathcal{J}^+ \rangle = 3/2 \quad (\text{C21})$$

$$\langle \mathcal{J}^+ | Q_i^2 | \mathcal{J}^+ \rangle = 3 \quad \langle \mathcal{J}^+ | \mathbf{S}_i \cdot \mathbf{S}_j | \mathcal{J}^+ \rangle = -3/2 \quad (\text{C22})$$

$$\langle \mathcal{J}^{++} | Q_i Q_j | \mathcal{J}^{++} \rangle = 1 \quad \langle \mathcal{J}^{++} | Q_i Q_j \mathbf{S}_i \cdot \mathbf{S}_j | \mathcal{J}^{++} \rangle = 1/4 \quad (\text{C23})$$

$$\langle \mathcal{J}^{++} | J_\pm^i J_\mp^j | \mathcal{J}^{++} \rangle = -2 \quad \langle \mathcal{J}^{++} | J_\pm^i J_\mp^j \mathbf{S}_i \cdot \mathbf{S}_j | \mathcal{J}^{++} \rangle = 5/2 \quad (\text{C24})$$

$$\langle \mathcal{J}^{++} | Q_i^2 | \mathcal{J}^{++} \rangle = 2 \quad \langle \mathcal{J}^{++} | \mathbf{S}_i \cdot \mathbf{S}_j | \mathcal{J}^{++} \rangle = -3/2 \quad (\text{C25})$$

The negatively-charged baryons have the same matrix elements as the corresponding positively-charged baryons.

One can see that these matrix elements are consistent with gauge invariance in the electroweak-symmetric phase. The charge operators encode the contribution of the third $SU(2)_L$ force carrier, the W^3 , and the ladder operators encode the contributions of the W^1 and W^2 . When $m_{W,Z} = 0$, the off-diagonal elements in Eqs. (C17) and (C18) cancel between the $W^{1,2}$ and W^3 contributions, and this cancellation occurs independently for the operators with and without spin. Therefore, the neutral $SU(2)_L$ eigenstates are mass eigenstates in this limit, as required. Moreover, observing the second diagonal entries for the neutral baryon matrices (corresponding to the neutral component of the baryon 5-plet) and the matrix elements for the charged baryons, the sum of the $W^{1,2}$ and W^3 contributions is identical for each 5-plet baryon. This is again true for the operators with and without spin independently. Therefore, the baryon 5-plet is exactly mass-degenerate in the symmetric phase, as required by gauge invariance. These observations are an important check on the validity of our approach and are true regardless of the spatial expectation value computation.

In the (2, 4) model,

$$\langle J^0 | Q_i Q_j | J^0 \rangle = \begin{pmatrix} -5/4 & 1 \\ 1 & -5/4 \end{pmatrix} \quad \langle J^0 | Q_i Q_j \mathbf{S}_i \cdot \mathbf{S}_j | J^0 \rangle = \begin{pmatrix} 15/16 & -3/4 \\ -3/4 & 15/16 \end{pmatrix} \quad (\text{C26})$$

$$\langle J^0 | J_\pm^i J_\mp^j | J^0 \rangle = \begin{pmatrix} -5/2 & -1 \\ -1 & 1/2 \end{pmatrix} \quad \langle J^0 | J_\pm^i J_\mp^j \mathbf{S}_i \cdot \mathbf{S}_j | J^0 \rangle = \begin{pmatrix} 15/8 & 3/4 \\ 3/4 & -3/8 \end{pmatrix} \quad (\text{C27})$$

$$\langle J^0 | Q_i^2 | J^0 \rangle = \begin{pmatrix} 5/2 & -2 \\ -2 & 5/2 \end{pmatrix} \quad \langle J^0 | \mathbf{S}_i \cdot \mathbf{S}_j | J^0 \rangle = \begin{pmatrix} -3/4 & 0 \\ 0 & -3/4 \end{pmatrix} \quad (\text{C28})$$

$$\langle J^+ | Q_i Q_j | J^+ \rangle = -3/4 \quad \langle J^+ | Q_i Q_j \mathbf{S}_i \cdot \mathbf{S}_j | J^+ \rangle = 9/16 \quad (\text{C29})$$

$$\langle J^+ | J_\pm^i J_\mp^j | J^+ \rangle = 0 \quad \langle J^+ | J_\pm^i J_\mp^j \mathbf{S}_i \cdot \mathbf{S}_j | J^+ \rangle = 0 \quad (\text{C30})$$

$$\langle J^+ | Q_i^2 | J^+ \rangle = 5/2 \quad \langle J^+ | \mathbf{S}_i \cdot \mathbf{S}_j | J^+ \rangle = -3/4 \quad (\text{C31})$$

$$\langle J^{++} | Q_i Q_j | J^{++} \rangle = 3/4 \quad \langle J^{++} | Q_i Q_j \mathbf{S}_i \cdot \mathbf{S}_j | J^{++} \rangle = -9/16 \quad (\text{C32})$$

$$\langle J^{++} | J_\pm^i J_\mp^j | J^{++} \rangle = -3/2 \quad \langle J^{++} | J_\pm^i J_\mp^j \mathbf{S}_i \cdot \mathbf{S}_j | J^{++} \rangle = 9/8 \quad (\text{C33})$$

$$\langle J^{++} | Q_i^2 | J^{++} \rangle = 5/2 \quad \langle J^{++} | \mathbf{S}_i \cdot \mathbf{S}_j | J^{++} \rangle = -3/4 \quad (\text{C34})$$

The same observations of the $W^{1,2}$ and W^3 contributions as above show that these matrix elements are also consistent with gauge invariance.

The above matrix elements provide some insight into the expected hierarchy of baryon masses. In the limit $m_q \ll m_W$, the W^\pm can be integrated out, and the spin-flavor eigenstates become approximate mass eigenstates. A neutral spin-flavor eigenstate can have a larger $\sum_i Q_i^2$ than a charged spin-flavor eigenstate. Then, baryon mass splittings can be dominated by quark mass splittings, and a charged baryon can be lighter than a neutral baryon.

Even when quark mass splitting do not dominate baryon mass splittings, differences in these matrix elements can cause charged states to be lighter than neutral states when $m_q \lesssim m_W$. Note for example the $Q_i Q_j$ and $J_\pm^i J_\mp^j$ matrix elements in the (2,4) model. The W^\pm contributions to the potential cancel for the singly-charged states and not for the neutral states. So when m_W is non-negligible and the electroweak inter-quark potentials are dominated by the photon, the potential is deeper for the singly-charged state than the heavier of the neutral states.

In the limit $m_q \gg m_W$, electroweak symmetry appears approximately restored in the dark sector, so the Q_i^2 contributions to the quark mass splittings nearly cancel, and the 5-plet baryons are approximately mass-degenerate. Then, in the effective field theory of baryons rather than quarks, electroweak self-energy corrections to baryons in a $(2J+1)$ -plet are proportional to the Casimir factor $J(J+1)$. Baryons in the 5-plets therefore receive larger self-energy corrections, so they are generically expected to be heavier than the singlet baryons in the large m_q limit.

As noted in Sec. II B, neutral states in adjacent odd $SU(2)_L$ representations (*i.e.* representations whose dimensions are odd and differ by two) are forbidden from mixing because they are eigenstates of the \mathcal{H} -parity transformation with opposite charges. In such cases, the lack of mixing is manifest in the mass calculation because the off-diagonal spin-flavor matrix elements that would mix these states vanish exactly.

4. Spatial Expectation Values

We use the variational method to estimate the spatial expectation values in the inter-quark potential with the template wavefunction in Eq. (5). We minimize baryon masses with respect to the k and k_1 parameters, thereby placing a bound on the ground state of the Hamiltonian. We are free to use any normalizable template function with appropriate boundary conditions, and the closer the ansatz is to the true solution of the Schrödinger equation, the better the estimate of the ground state. We chose a slight generalization of an exponentially-suppressed function, which is a typical qualitative form of bound state wavefunctions such as the ground state of the Hydrogen atom.

Expectation values of operators \mathcal{O} acting on baryon spatial states can be computed in the standard way

$$\langle \mathcal{O} \rangle = \frac{\int d^3 r_1 \cdots d^3 r_{N_c} \psi^* \mathcal{O} \psi}{\int d^3 r_1 \cdots d^3 r_{N_c} \psi^* \psi}. \quad (\text{C35})$$

However, integrating over all positions gives a volume factor in the numerator and denominator. The integrands are translationally invariant, so it is practical to choose an origin \mathbf{r}_0 (analogous to fixing the proton at the origin in the Hydrogen atom) and enforcing it with a delta function.

$$\langle \mathcal{O} \rangle = \frac{\int d^3 r_1 \cdots d^3 r_{N_c} \psi^* \mathcal{O} \psi \delta^{(3)}(\mathbf{r}_0)}{\int d^3 r_1 \cdots d^3 r_{N_c} \psi^* \psi \delta^{(3)}(\mathbf{r}_0)}. \quad (\text{C36})$$

The choice of origin is arbitrary, but it is convenient to choose $\mathbf{r}_0 = \mathbf{r}_{N_c}$. The required expectation values include those listed in Eq. (4), as well as the $\langle p_i^2 \rangle$ factor in the free Hamiltonian.

The spatial integrals in Eq. (C36) become increasingly challenging as N_c becomes large. For the two-body wavefunction (relevant for $N_c = 2$ baryons and all mesons), we analytically find

$$a_0 = \frac{8(4k^2 + 12k_1^2 + 6k_1 m_V + m_V^2 + 12kk_1 + 4km_V)}{(k^2 + 3kk_1 + 3k_1^2)(m_V/k + 2)^5} \quad (\text{C37})$$

$$a_1 = \frac{4k(4k^2 + 6k_1^2 + 4k_1 m_V + m_V^2 + 8kk_1 + 4km_V)}{(k^2 + 3kk_1 + 3k_1^2)(m_V/k + 2)^4} \quad (\text{C38})$$

$$a_2 = \frac{4k^2(4k^2 + 2k_1^2 + 2k_1 m_V + m_V^2 + 4kk_1 + 4km_V)}{(k^2 + 3kk_1 + 3k_1^2)(m_V/k + 2)^3} \quad (\text{C39})$$

$$b = \frac{4k(12k^4 + 20k^3 m_V - 6kk_1 m_V^2 + 2km_V^3 - 2k_1^2 m_V^2 - 2k_1 m_V^3 + 2k^2 k_1^2 - 4k^2 k_1 m_V + 11k^2 m_V^2)}{(k^2 + 3kk_1 + 3k_1^2)(m_V/k + 2)^4} \quad (\text{C40})$$

$$c_1 = -\frac{16(4k^3 + 8k^2 k_1 + 4k^2 m_V - 3k_1^2 m_V - k_1 m_V^2 + 6kk_1^2 + 2kk_1 m_V + km_V^2)}{(k^2 + 3kk_1 + 3k_1^2)(m_V/k + 2)^5} \quad (\text{C41})$$

$$c_2 = -\frac{8k(4k^3 + 4k^2k_1 + 4k^2m_V - 2k_1^2m_V - k_1m_V^2 + 2kk_1^2 + km_V^2)}{(k^2 + 3kk_1 + 3k_1^2)(m_V/k + 2)^4} \quad (\text{C42})$$

$$d_2 = -\frac{8k(4k^3 - 2kk_1m_V + km_V^2 + 4k^2k_1 + 4k^2m_V - 6k_1^2m_V - 2k_1m_V^2)}{(k^2 + 3kk_1 + 3k_1^2)(m_V/k + 2)^5} \quad (\text{C43})$$

$$d_3 = -\frac{4k^2(4k^3 + 4k^2m_V - 4k_1^2m_V - 2k_1m_V^2 - 2kk_1^2 - 4kk_1m_V + km_V^2)}{(k^2 + 3kk_1 + 3k_1^2)(m_V/k + 2)^4} \quad (\text{C44})$$

$$\delta = \frac{k^5}{\pi(k^2 + 3kk_1 + 3k_1^2)} \quad (\text{C45})$$

$$\langle p_i^2 \rangle = \frac{k^2(k^2 + kk_1 + k_1^2)}{k^2 + 3kk_1 + 3k_1^2}. \quad (\text{C46})$$

Note that the denominators above contain identical normalization factors, and integrals whose integrands are quadratic in ψ must be quadratic in k_1 . For greater than two bodies, we resort to numerical computation. For the expectation values that do not depend on m_V , the dimensionful scale k can be factored out of the integrand, and one can perform a scale-free numerical integral for the terms constant, linear, and quadratic in k_1 .

For the expectation values that do depend on m_V , factoring out k from the integrand leaves a dependence on the ratio m_V/k . With some insight from the integrals we can perform analytically, we can make an ansatz for how the integrals depend on m_V/k . Each matrix element we have computed analytically (some of which are feasible with three bodies) organizes itself into a sum of Laurent series in m_V/k with particular pole structures. The poles are at $m_V/k = -2$ for two bodies and $m_V/k = -4$ for three bodies. While unphysical, this analytic structure at negative values of m_V/k helps us predict forms of the integrals for baryons with larger N_c . To understand why these poles appear, consider the integrand for computing a_0 with $k_1 = 0$ for three bodies

$$a_0 = \langle e^{-m_V|\mathbf{r}_1 - \mathbf{r}_3|} \rangle \propto \int d^3r_1 d^3r_2 d^3r_3 e^{-m_V|\mathbf{r}_1 - \mathbf{r}_3|} |\psi|^2 \delta^{(3)}(\mathbf{r}_3) \propto \int d^3u_1 d^3u_2 e^{-(m_V/k)u_1 - 2(|\mathbf{u}_1 - \mathbf{u}_2| + u_1 + u_2)}, \quad (\text{C47})$$

where $\mathbf{u}_i = k\mathbf{r}_i$ is a dimensionless spatial variable. This integral is singular when the argument of the exponent has non-negative real part. If one evaluates the \mathbf{u}_1 integral while holding \mathbf{u}_2 fixed, the m_V -independent part of the exponent scales like $-4u_1$, and there is a singularity in the limit $m_V/k \rightarrow -4$. This argument provides some intuition as to why the poles in the analytical solutions appear at specific values of m_V/k . Moreover, we can extend this intuition to N_c bodies, for which the m_V -independent part of the exponent scales like $-2(N_c - 1)u_1$ holding the other variables constant, so we expect a pole in the above expectation values at $m_V/k = -2(N_c - 1)$.

For $N_c > 3$, the integrals may acquire additional poles at negative values of m_V/k that are further from zero than $-2(N_c - 1)$. This is because there are more complicated integration trajectories that give rise to a singularity. For $N_c = 4$, consider

$$a_0 \propto \int d^3u_1 d^3u_2 d^3u_3 e^{-(m_V/k)u_1 - 2(|\mathbf{u}_1 - \mathbf{u}_2| + |\mathbf{u}_1 - \mathbf{u}_3| + |\mathbf{u}_2 - \mathbf{u}_3| + u_1 + u_2 + u_3)} \quad (\text{C48})$$

when $k_1 = 0$. Holding \mathbf{u}_3 fixed and integrating along the trajectory with $\mathbf{u}_2 = \mathbf{u}_1$, the m_V -independent part of the exponent scales like $-8u_1$, which suggests a pole at $m_V/k = -8$ in addition to the pole at $m_V/k = -6$ identified above. By contrast, for the $N_c = 3$ case, integrating along the trajectory $\mathbf{u}_2 = \mathbf{u}_1$ suggests a pole at $m_V/k = -4$ (identical to the pole found above), so there is no reason to expect more than one pole in the three-body integrals. Likewise, integrating along the $\mathbf{u}_3 = \mathbf{u}_2 = \mathbf{u}_1$ trajectory in the four-body integral suggests the same pole at $m_V/k = -6$ as identified above. When $N_c > 4$, even more poles may appear, but these become more negative and therefore have more suppressed contributions for physically relevant values of m_V/k as N_c increases.

In our analysis with $N_c = 4$, we estimate the m_V -dependence of the spatial expectation values by numerically integrating with many values of m_V and performing fits to sums of Laurent series with strictly negative powers centered at each of the two expected poles

$$\langle \mathcal{O} \rangle = \sum_{n=n_{\min}}^{n_{\max}} \sum_{x \in \text{poles}} \frac{f_{n,x}}{(m_V/k - x)^n}, \quad (\text{C49})$$

where $f_{n,x}$ are fit coefficients. We do this for terms constant, linear, and quadratic in k_1 independently. To decide which terms to include in the Laurent series (set by n_{\min} and n_{\max} in Eq. (C49)), we again take inspiration from the

two- and three-body analytical integrals. In particular, we conjecture that in the large- m_V limit, where the series in Eq. (C49) is dominated by terms with $n = n_{\min}$, any particular spatial matrix element decreases in magnitude with respect to m_V equally quickly for all values of N_c . For example, $a_0 \sim 1/m_V^3$ for large m_V when $N_c \in \{2, 3\}$, so we assume this is true for all N_c . This conjecture fixes n_{\min} and is sensible because if the decrease in m_V were slower, the contribution of the term to the potential in Eq. (3) may *increase* with m_V , which is clearly unphysical. To fix n_{\max} , we observe that when N_c increases by one, there is an additional radial integral in the expectation value computation, which contributes an additional factor of r_i^2 . These two powers of r_i lead to two additional powers of m_V in the denominator, so we conjecture

$$n_{\max} = 2(N_c - 2) + n_{\max}^{N_c=2}, \quad (\text{C50})$$

where $n_{\max}^{N_c=2}$ is the two-body value of n_{\max} . We find good numerical agreement with this approach.

We can check for self-consistency in our estimates of these integrals by noting that some of the spatial expectation values are inter-related by derivatives:

$$a_0 = -\frac{\partial a_1}{\partial m_V} \quad a_1 = -\frac{\partial a_2}{\partial m_V} \quad (\text{C51})$$

$$c_1 = -\frac{\partial c_2}{\partial m_V} \quad d_2 = -\frac{\partial d_3}{\partial m_V}. \quad (\text{C52})$$

We found that our estimates of a_n and c_n agreed well with these relations. For d_3 with $N_c = 4$, we encountered difficulties in the convergence of the numerical integrals, so we found our estimate of d_3 by anti-differentiating our estimate of d_2 . Note that these derivatives are consistent with our conjectures for n_{\min} and n_{\max} .

We can now express the hadron mass operator as a matrix acting on the space of hadron $SU(2)_L$ eigenstates that depends on k and k_1 . For the variational method, we estimate the ground state by minimizing the mass with respect to k and k_1 . One remaining question is the renormalization scale μ at which to evaluate the running couplings that appear in the inter-quark potential. To answer this question, we identify the characteristic hadron length scale (the ‘‘Bohr radius’’) as $1/k$, as this sets the exponential decay rate of the spatial wavefunction in Eq. (5). We therefore identify the hadron’s characteristic energy scale as k and evaluate the running couplings at $\mu = k$. We use the one-loop renormalization group evolution of α_χ in the effective field theory with the dark quarks integrated out [135]

$$\alpha_\chi(\mu) = \frac{6\pi}{11N_c \ln(\mu/\Lambda_\chi)}. \quad (\text{C53})$$

We also run α_W and α_{EM} at one loop in the effective field theory without the Higgs or top quark when $\mu < m_Z$ and with the full SM when $\mu > m_Z$ (neglecting threshold effects) [128]. The running of α_W and α_{EM} has a very small impact.

If one tries to minimize the mass with respect to k while using $\mu = k$ in the running couplings, Eq. (C53) shows that one encounters unphysical large logarithms that disrupt the minimization procedure. We therefore implement an iterative minimization approach. We start with an initial hypothesis for the inverse Bohr radius of $k \simeq \alpha_\chi(k) m_q$, which is solved by

$$k \simeq \frac{6\pi m_q}{11N_c \mathcal{W}\left(\frac{6\pi m_q}{11N_c \Lambda_\chi}\right)}, \quad (\text{C54})$$

where \mathcal{W} is the principal branch of the Lambert W function (also known as the product logarithm) [136]. We evaluate the couplings in the inter-quark potential with μ equal to this hypothesized k , minimize with respect to the k and k_1 that appear in the spatial expectation values, use the value of k corresponding to that minimum as the new hypothesis for μ , then repeat the minimization in this way until the minimized mass converges. This procedure ensures the couplings are evaluated at the inverse Bohr radius while avoiding large logarithms in their renormalization group evolution.

Performing the minimization procedure described in above is straightforward for hadron states that are not mixed by the mass operator (*e.g.* the charged states in the (2, 4) and (4, 3) models). These are simultaneous $SU(2)_L$ and mass eigenstates, and each will have its own optimal k and k_1 . However, there is an ambiguity in the minimization calculation when the mass operator has off-diagonal elements. Consider the 2×2 mass matrix in the basis of the neutral $SU(2)_L$ eigenstates in the (2, 4) or (4, 3) model. Each matrix element is a function of k and k_1 , as is each mass

eigenvalue and the mixing angle between the $SU(2)_L$ eigenstates. If we simply minimized each mass eigenvalue with respect to its own k and k_1 individually, each value of the optimization parameters corresponds to a distinct set of eigenvectors. If the mass eigenstates are evaluated with different values of k and k_1 , those states are not orthogonal. In other words, the mixing angle is ill-defined if there are different values of k and k_1 used for the two mass eigenvalues.

We resolve this ambiguity by performing the minimization in multiple ways. We start by minimizing the lesser mass eigenvalue and using the optimal k and k_1 values to find the greater mass eigenvalue and mass eigenstates. We then do the reverse, minimizing the greater eigenvalue and using the corresponding optimization parameters to evaluate the lesser eigenvalue and eigenstates. The differences between the masses and mixing angles computed using each method represents uncertainties in the calculation. This uncertainty in the DM mass is around 0.1% for the (2, 4) model and 0.001% for the (4, 3) model. The resulting uncertainty in $|\langle m_{\text{DM}} | 5\text{-plet} \rangle|^2$ is $\mathcal{O}(10\%)$, which shifts the steep drop-off shown in Fig. 1 by less than half an order-of-magnitude in m_q .

-
- [1] M. Cirelli, A. Strumia, and J. Zupan, “Dark Matter,” [arXiv:2406.01705 \[hep-ph\]](#).
- [2] C. Kilic, T. Okui, and R. Sundrum, “Vectorlike Confinement at the LHC,” *JHEP* **02** (2010) 018, [arXiv:0906.0577 \[hep-ph\]](#).
- [3] Y. Bai and R. J. Hill, “Weakly Interacting Stable Pions,” *Phys. Rev. D* **82** (2010) 111701, [arXiv:1005.0008 \[hep-ph\]](#).
- [4] O. Antipin, M. Redi, and A. Strumia, “Dynamical generation of the weak and Dark Matter scales from strong interactions,” *JHEP* **01** (2015) 157, [arXiv:1410.1817 \[hep-ph\]](#).
- [5] T. Appelquist *et al.*, “Stealth Dark Matter: Dark scalar baryons through the Higgs portal,” *Phys. Rev. D* **92** no. 7, (2015) 075030, [arXiv:1503.04203 \[hep-ph\]](#).
- [6] A. Mitridate, M. Redi, J. Smirnov, and A. Strumia, “Dark Matter as a weakly coupled Dark Baryon,” *JHEP* **10** (2017) 210, [arXiv:1707.05380 \[hep-ph\]](#).
- [7] G. D. Kribs, A. Martin, and T. Tong, “Effective Theories of Dark Mesons with Custodial Symmetry,” *JHEP* **08** (2019) 020, [arXiv:1809.10183 \[hep-ph\]](#).
- [8] G. D. Kribs, A. Martin, B. Ostdiek, and T. Tong, “Dark Mesons at the LHC,” *JHEP* **07** (2019) 133, [arXiv:1809.10184 \[hep-ph\]](#).
- [9] T. Abe, R. Sato, and T. Yamanaka, “Composite Dark Matter with Forbidden Annihilation,” [arXiv:2404.03963 \[hep-ph\]](#).
- [10] P. Asadi, G. D. Kribs, and C. J. H. Mantel, “Direct Detection of Dark Baryons Naturally Suppressed by \mathcal{H} -parity,” [arXiv:2410.23631 \[hep-ph\]](#).
- [11] R. Essig, “Direct Detection of Non-Chiral Dark Matter,” *Phys. Rev. D* **78** (2008) 015004, [arXiv:0710.1668 \[hep-ph\]](#).
- [12] J. Hisano, K. Ishiwata, and N. Nagata, “A complete calculation for direct detection of Wino dark matter,” *Phys. Lett. B* **690** (2010) 311–315, [arXiv:1004.4090 \[hep-ph\]](#).
- [13] R. J. Hill and M. P. Solon, “Standard Model anatomy of WIMP dark matter direct detection I: weak-scale matching,” *Phys. Rev. D* **91** (2015) 043504, [arXiv:1401.3339 \[hep-ph\]](#).
- [14] R. J. Hill and M. P. Solon, “Standard Model anatomy of WIMP dark matter direct detection II: QCD analysis and hadronic matrix elements,” *Phys. Rev. D* **91** (2015) 043505, [arXiv:1409.8290 \[hep-ph\]](#).
- [15] C.-Y. Chen, R. J. Hill, M. P. Solon, and A. M. Wijangco, “Power Corrections to the Universal Heavy WIMP-Nucleon Cross Section,” *Phys. Lett. B* **781** (2018) 473–479, [arXiv:1801.08551 \[hep-ph\]](#).
- [16] S. Bottaro, D. Buttazzo, M. Costa, R. Franceschini, P. Panci, D. Redigolo, and L. Vittorio, “Closing the window on WIMP Dark Matter,” *Eur. Phys. J. C* **82** no. 1, (2022) 31, [arXiv:2107.09688 \[hep-ph\]](#).
- [17] S. Bottaro, D. Buttazzo, M. Costa, R. Franceschini, P. Panci, D. Redigolo, and L. Vittorio, “The last complex WIMPs standing,” *Eur. Phys. J. C* **82** no. 11, (2022) 992, [arXiv:2205.04486 \[hep-ph\]](#).
- [18] Q. Chen, G.-J. Ding, and R. J. Hill, “General heavy WIMP nucleon elastic scattering,” *Phys. Rev. D* **108** no. 11, (2023) 116023, [arXiv:2309.02715 \[hep-ph\]](#).
- [19] I. M. Bloch, S. Bottaro, D. Redigolo, and L. Vittorio, “Looking for WIMPs through the neutrino fogs,” [arXiv:2410.02723 \[hep-ph\]](#).
- [20] M. J. Strassler and K. M. Zurek, “Echoes of a hidden valley at hadron colliders,” *Phys. Lett. B* **651** (2007) 374–379, [arXiv:hep-ph/0604261](#).
- [21] T. Han, Z. Si, K. M. Zurek, and M. J. Strassler, “Phenomenology of hidden valleys at hadron colliders,” *JHEP* **07** (2008) 008, [arXiv:0712.2041 \[hep-ph\]](#).
- [22] J. Kang and M. A. Luty, “Macroscopic Strings and ‘Quirks’ at Colliders,” *JHEP* **11** (2009) 065, [arXiv:0805.4642 \[hep-ph\]](#).
- [23] J. E. Juknevich, D. Melnikov, and M. J. Strassler, “A Pure-Glue Hidden Valley I. States and Decays,” *JHEP* **07** (2009) 055, [arXiv:0903.0883 \[hep-ph\]](#).
- [24] G. D. Kribs, T. S. Roy, J. Terning, and K. M. Zurek, “Quirky Composite Dark Matter,” *Phys. Rev. D* **81** (2010) 095001, [arXiv:0909.2034 \[hep-ph\]](#).
- [25] J. E. Juknevich, “Pure-gluon hidden valleys through the Higgs portal,” *JHEP* **08** (2010) 121, [arXiv:0911.5616 \[hep-ph\]](#).
- [26] R. Harnik, G. D. Kribs, and A. Martin, “Quirks at the Tevatron and Beyond,” *Phys. Rev. D* **84** (2011) 035029, [arXiv:1106.2569 \[hep-ph\]](#).
- [27] M. Frigerio, A. Pomarol, F. Riva, and A. Urbano, “Composite Scalar Dark Matter,” *JHEP* **07** (2012) 015, [arXiv:1204.2808 \[hep-ph\]](#).
- [28] P. Schwaller, D. Stolarski, and A. Weiler, “Emerging Jets,” *JHEP* **05** (2015) 059, [arXiv:1502.05409 \[hep-ph\]](#).
- [29] T. Cohen, M. Lisanti, and H. K. Lou, “Semivisible Jets: Dark Matter Undercover at the LHC,” *Phys. Rev. Lett.* **115** no. 17, (2015) 171804, [arXiv:1503.00009 \[hep-ph\]](#).
- [30] A. Carmona and M. Chala, “Composite Dark Sectors,” *JHEP* **06** (2015) 105, [arXiv:1504.00332 \[hep-ph\]](#).
- [31] S. Knapen, S. Pagan Griso, M. Papucci, and D. J. Robinson, “Triggering Soft Bombs at the LHC,” *JHEP* **08** (2017) 076, [arXiv:1612.00850 \[hep-ph\]](#).
- [32] S. Knapen, H. K. Lou, M. Papucci, and J. Setford, “Tracking down Quirks at the Large Hadron Collider,” *Phys. Rev. D* **96** no. 11, (2017) 115015, [arXiv:1708.02243 \[hep-ph\]](#).
- [33] J. A. Evans and M. A. Luty, “Stopping Quirks at the LHC,” *JHEP* **06** (2019) 090, [arXiv:1811.08903 \[hep-ph\]](#).
- [34] E. Bernreuther, F. Kahlhoefer, M. Krämer, and P. Tunney, “Strongly interacting dark sectors in the early Universe and at the LHC through a simplified portal,” *JHEP* **01** (2020) 162, [arXiv:1907.04346 \[hep-ph\]](#).

- [35] E. Bernreuther, T. Finke, F. Kahlhoefer, M. Krämer, and A. Mück, “Casting a graph net to catch dark showers,” *SciPost Phys.* **10** no. 2, (2021) 046, [arXiv:2006.08639 \[hep-ph\]](#).
- [36] S. Knapen, J. Shelton, and D. Xu, “Perturbative benchmark models for a dark shower search program,” *Phys. Rev. D* **103** no. 11, (2021) 115013, [arXiv:2103.01238 \[hep-ph\]](#).
- [37] J. Barron, D. Curtin, G. Kasieczka, T. Plehn, and A. Spourdalakis, “Unsupervised hadronic SUEP at the LHC,” *JHEP* **12** (2021) 129, [arXiv:2107.12379 \[hep-ph\]](#).
- [38] T. Kuwahara and S.-R. Yuan, “Dark vector mesons at LHC forward detector searches,” *JHEP* **06** (2023) 208, [arXiv:2303.03736 \[hep-ph\]](#).
- [39] A. Batz, T. Cohen, D. Curtin, C. Gemell, and G. D. Kribs, “Dark sector glueballs at the LHC,” *JHEP* **04** (2024) 070, [arXiv:2310.13731 \[hep-ph\]](#).
- [40] J. Bagnasco, M. Dine, and S. D. Thomas, “Detecting technibaryon dark matter,” *Phys. Lett. B* **320** (1994) 99–104, [arXiv:hep-ph/9310290](#).
- [41] D. S. M. Alves, S. R. Behbahani, P. Schuster, and J. G. Wacker, “Composite Inelastic Dark Matter,” *Phys. Lett. B* **692** (2010) 323–326, [arXiv:0903.3945 \[hep-ph\]](#).
- [42] D. Spier Moreira Alves, S. R. Behbahani, P. Schuster, and J. G. Wacker, “The Cosmology of Composite Inelastic Dark Matter,” *JHEP* **06** (2010) 113, [arXiv:1003.4729 \[hep-ph\]](#).
- [43] M. R. Buckley and E. T. Neil, “Thermal dark matter from a confining sector,” *Phys. Rev. D* **87** no. 4, (2013) 043510, [arXiv:1209.6054 \[hep-ph\]](#).
- [44] S. Bhattacharya, B. Melić, and J. Wudka, “Pionic Dark Matter,” *JHEP* **02** (2014) 115, [arXiv:1307.2647 \[hep-ph\]](#).
- [45] O. Antipin, M. Redi, A. Strumia, and E. Vigiani, “Accidental Composite Dark Matter,” *JHEP* **07** (2015) 039, [arXiv:1503.08749 \[hep-ph\]](#).
- [46] E. Hardy, R. Lasenby, J. March-Russell, and S. M. West, “Signatures of Large Composite Dark Matter States,” *JHEP* **07** (2015) 133, [arXiv:1504.05419 \[hep-ph\]](#).
- [47] V. De Luca, A. Mitridate, M. Redi, J. Smirnov, and A. Strumia, “Colored Dark Matter,” *Phys. Rev. D* **97** no. 11, (2018) 115024, [arXiv:1801.01135 \[hep-ph\]](#).
- [48] R. Contino, A. Podo, and F. Revello, “Composite Dark Matter from Strongly-Interacting Chiral Dynamics,” *JHEP* **02** (2021) 091, [arXiv:2008.10607 \[hep-ph\]](#).
- [49] W. Detmold, M. McCullough, and A. Pochinsky, “Dark Nuclei I: Cosmology and Indirect Detection,” *Phys. Rev. D* **90** no. 11, (2014) 115013, [arXiv:1406.2276 \[hep-ph\]](#).
- [50] A. Soni and Y. Zhang, “Hidden SU(N) Glueball Dark Matter,” *Phys. Rev. D* **93** no. 11, (2016) 115025, [arXiv:1602.00714 \[hep-ph\]](#).
- [51] R. Mahbubani, M. Redi, and A. Tesi, “Indirect detection of composite asymmetric dark matter,” *Phys. Rev. D* **101** no. 10, (2020) 103037, [arXiv:1908.00538 \[hep-ph\]](#).
- [52] J. M. Cline, Z. Liu, G. D. Moore, and W. Xue, “Composite strongly interacting dark matter,” *Phys. Rev. D* **90** no. 1, (2014) 015023, [arXiv:1312.3325 \[hep-ph\]](#).
- [53] K. K. Boddy, J. L. Feng, M. Kaplinghat, and T. M. P. Tait, “Self-Interacting Dark Matter from a Non-Abelian Hidden Sector,” *Phys. Rev. D* **89** no. 11, (2014) 115017, [arXiv:1402.3629 \[hep-ph\]](#).
- [54] G. Krnjaic and K. Sigurdson, “Big Bang Darkleosynthesis,” *Phys. Lett. B* **751** (2015) 464–468, [arXiv:1406.1171 \[hep-ph\]](#).
- [55] M. A. Buen-Abad, G. Marques-Tavares, and M. Schmaltz, “Non-Abelian dark matter and dark radiation,” *Phys. Rev. D* **92** no. 2, (2015) 023531, [arXiv:1505.03542 \[hep-ph\]](#).
- [56] C. Gross, A. Mitridate, M. Redi, J. Smirnov, and A. Strumia, “Cosmological Abundance of Colored Relics,” *Phys. Rev. D* **99** no. 1, (2019) 016024, [arXiv:1811.08418 \[hep-ph\]](#).
- [57] L. Morrison, S. Profumo, and D. J. Robinson, “Large N -ightmare Dark Matter,” *JCAP* **05** (2021) 058, [arXiv:2010.03586 \[hep-ph\]](#).
- [58] R. Contino, K. Max, and R. K. Mishra, “Searching for elusive dark sectors with terrestrial and celestial observations,” *JHEP* **06** (2021) 127, [arXiv:2012.08537 \[hep-ph\]](#).
- [59] R. Garani, M. Redi, and A. Tesi, “Dark QCD matters,” *JHEP* **12** (2021) 139, [arXiv:2105.03429 \[hep-ph\]](#).
- [60] R. Krall and M. Reece, “Last Electroweak WIMP Standing: Pseudo-Dirac Higgsino Status and Compact Stars as Future Probes,” *Chin. Phys. C* **42** no. 4, (2018) 043105, [arXiv:1705.04843 \[hep-ph\]](#).
- [61] A. De Rujula, H. Georgi, and S. L. Glashow, “Hadron Masses in a Gauge Theory,” *Phys. Rev. D* **12** (1975) 147–162.
- [62] A. Manohar and H. Georgi, “Chiral Quarks and the Nonrelativistic Quark Model,” *Nucl. Phys. B* **234** (1984) 189–212.
- [63] H. Georgi, *Weak Interactions and Modern Particle Theory*. 1984.
- [64] M. De Sanctis, “A generalization of the Fermi-Breit equation to non-Coulombic spatial interactions,” *Eur. Phys. J. A* **41** (2009) 169–178.
- [65] M. Cirelli, N. Fornengo, and A. Strumia, “Minimal dark matter,” *Nucl. Phys. B* **753** (2006) 178–194, [arXiv:hep-ph/0512090](#).
- [66] W. Detmold, M. McCullough, and A. Pochinsky, “Dark nuclei. II. Nuclear spectroscopy in two-color QCD,” *Phys. Rev. D* **90** no. 11, (2014) 114506, [arXiv:1406.4116 \[hep-lat\]](#).
- [67] **LZ Collaboration** Collaboration, J. Aalbers *et al.*, “Dark Matter Search Results from 4.2 Tonne-Years of Exposure of the LUX-ZEPLIN (LZ) Experiment,” [arXiv:2410.17036 \[hep-ex\]](#).
- [68] **XENON Collaboration**, E. Aprile *et al.*, “Physics reach of the XENON1T dark matter experiment,” *JCAP* **04** (2016) 027, [arXiv:1512.07501 \[physics.ins-det\]](#).
- [69] C. Blanco, Y. Kahn, B. Lillard, and S. D. McDermott, “Dark Matter Daily Modulation With Anisotropic Organic

- Crystals,” *Phys. Rev. D* **104** (2021) 036011, [arXiv:2103.08601 \[hep-ph\]](#).
- [70] C. Blanco, I. Harris, Y. Kahn, B. Lillard, and J. Pérez-Ríos, “Molecular Migdal effect,” *Phys. Rev. D* **106** no. 11, (2022) 115015, [arXiv:2208.09002 \[hep-ph\]](#).
- [71] D. Tucker-Smith and N. Weiner, “Inelastic dark matter,” *Phys. Rev. D* **64** (2001) 043502, [arXiv:hep-ph/0101138](#).
- [72] S. Chang, N. Weiner, and I. Yavin, “Magnetic Inelastic Dark Matter,” *Phys. Rev. D* **82** (2010) 125011, [arXiv:1007.4200 \[hep-ph\]](#).
- [73] K. Kumar, A. Menon, and T. M. P. Tait, “Magnetic Fluffy Dark Matter,” *JHEP* **02** (2012) 131, [arXiv:1111.2336 \[hep-ph\]](#).
- [74] J. Eby, P. J. Fox, and G. D. Kribs, “Earth-Catalyzed Detection of Magnetic Inelastic Dark Matter with Photons in Large Underground Detectors,” [arXiv:2312.08478 \[hep-ph\]](#).
- [75] G. Ovanessian and L. Vecchi, “Direct detection of dark matter polarizability,” *JHEP* **07** (2015) 128, [arXiv:1410.0601 \[hep-ph\]](#).
- [76] B. J. Kavanagh, P. Panci, and R. Ziegler, “Faint Light from Dark Matter: Classifying and Constraining Dark Matter-Photon Effective Operators,” *JHEP* **04** (2019) 089, [arXiv:1810.00033 \[hep-ph\]](#).
- [77] P. Asadi, E. D. Kramer, E. Kuflik, G. W. Ridgway, T. R. Slatyer, and J. Smirnov, “Thermal squeezeout of dark matter,” *Phys. Rev. D* **104** no. 9, (2021) 095013, [arXiv:2103.09827 \[hep-ph\]](#).
- [78] P. Asadi, E. D. Kramer, E. Kuflik, G. W. Ridgway, T. R. Slatyer, and J. Smirnov, “Accidentally Asymmetric Dark Matter,” *Phys. Rev. Lett.* **127** no. 21, (2021) 211101, [arXiv:2103.09822 \[hep-ph\]](#).
- [79] P. Asadi, E. D. Kramer, E. Kuflik, T. R. Slatyer, and J. Smirnov, “Glueballs in a thermal squeezeout model,” *JHEP* **07** (2022) 006, [arXiv:2203.15813 \[hep-ph\]](#).
- [80] B. Svetitsky and L. G. Yaffe, “Critical Behavior at Finite Temperature Confinement Transitions,” *Nucl. Phys. B* **210** (1982) 423–447.
- [81] C. Alexandrou, A. Borici, A. Feo, P. de Forcrand, A. Galli, F. Jegerlehner, and T. Takaishi, “The Deconfinement phase transition in one flavor QCD,” *Phys. Rev. D* **60** (1999) 034504, [arXiv:hep-lat/9811028](#).
- [82] O. Kaczmarek, F. Karsch, E. Laermann, and M. Lutgemeier, “Heavy quark potentials in quenched QCD at high temperature,” *Phys. Rev. D* **62** (2000) 034021, [arXiv:hep-lat/9908010](#).
- [83] B. Lucini, M. Teper, and U. Wenger, “The High temperature phase transition in SU(N) gauge theories,” *JHEP* **01** (2004) 061, [arXiv:hep-lat/0307017](#).
- [84] B. Lucini, M. Teper, and U. Wenger, “Properties of the deconfining phase transition in SU(N) gauge theories,” *JHEP* **02** (2005) 033, [arXiv:hep-lat/0502003](#).
- [85] Y. Aoki, G. Endrodi, Z. Fodor, S. D. Katz, and K. K. Szabo, “The Order of the quantum chromodynamics transition predicted by the standard model of particle physics,” *Nature* **443** (2006) 675–678, [arXiv:hep-lat/0611014](#).
- [86] **WHOT-QCD** Collaboration, H. Saito, S. Ejiri, S. Aoki, T. Hatsuda, K. Kanaya, Y. Maezawa, H. Ohno, and T. Umeda, “Phase structure of finite temperature QCD in the heavy quark region,” *Phys. Rev. D* **84** (2011) 054502, [arXiv:1106.0974 \[hep-lat\]](#). [Erratum: *Phys.Rev.D* 85, 079902 (2012)].
- [87] I. Goldman and S. Nussinov, “Weakly Interacting Massive Particles and Neutron Stars,” *Phys. Rev. D* **40** (1989) 3221–3230.
- [88] A. Gould, B. T. Draine, R. W. Romani, and S. Nussinov, “Neutron Stars: Graveyard of Charged Dark Matter,” *Phys. Lett. B* **238** (1990) 337–343.
- [89] C. Kouvaris and P. Tinyakov, “Can Neutron stars constrain Dark Matter?,” *Phys. Rev. D* **82** (2010) 063531, [arXiv:1004.0586 \[astro-ph.GA\]](#).
- [90] A. de Lavallaz and M. Fairbairn, “Neutron Stars as Dark Matter Probes,” *Phys. Rev. D* **81** (2010) 123521, [arXiv:1004.0629 \[astro-ph.GA\]](#).
- [91] S. D. McDermott, H.-B. Yu, and K. M. Zurek, “Constraints on Scalar Asymmetric Dark Matter from Black Hole Formation in Neutron Stars,” *Phys. Rev. D* **85** (2012) 023519, [arXiv:1103.5472 \[hep-ph\]](#).
- [92] C. Kouvaris and P. Tinyakov, “Excluding Light Asymmetric Bosonic Dark Matter,” *Phys. Rev. Lett.* **107** (2011) 091301, [arXiv:1104.0382 \[astro-ph.CO\]](#).
- [93] T. Güver, A. E. Erkoca, M. Hall Reno, and I. Sarcevic, “On the capture of dark matter by neutron stars,” *JCAP* **05** (2014) 013, [arXiv:1201.2400 \[hep-ph\]](#).
- [94] C. Kouvaris and P. Tinyakov, “Growth of Black Holes in the interior of Rotating Neutron Stars,” *Phys. Rev. D* **90** no. 4, (2014) 043512, [arXiv:1312.3764 \[astro-ph.SR\]](#).
- [95] J. Bramante and T. Linden, “Detecting Dark Matter with Imploding Pulsars in the Galactic Center,” *Phys. Rev. Lett.* **113** no. 19, (2014) 191301, [arXiv:1405.1031 \[astro-ph.HE\]](#).
- [96] J. Bramante, A. Delgado, and A. Martin, “Multiscatter stellar capture of dark matter,” *Phys. Rev. D* **96** no. 6, (2017) 063002, [arXiv:1703.04043 \[hep-ph\]](#).
- [97] C. Kouvaris, P. Tinyakov, and M. H. G. Tytgat, “NonPrimordial Solar Mass Black Holes,” *Phys. Rev. Lett.* **121** no. 22, (2018) 221102, [arXiv:1804.06740 \[astro-ph.HE\]](#).
- [98] R. Garani, Y. Genolini, and T. Hambye, “New Analysis of Neutron Star Constraints on Asymmetric Dark Matter,” *JCAP* **05** (2019) 035, [arXiv:1812.08773 \[hep-ph\]](#).
- [99] S. A. R. Ellis, “Premature black hole death of Population III stars by dark matter,” *JCAP* **05** no. 05, (2022) 025, [arXiv:2111.02414 \[astro-ph.CO\]](#).
- [100] S. Bhattacharya, B. Dasgupta, R. Laha, and A. Ray, “Can LIGO Detect Nonannihilating Dark Matter?,” *Phys. Rev. Lett.* **131** no. 9, (2023) 091401, [arXiv:2302.07898 \[hep-ph\]](#).
- [101] N. F. Bell, A. Melatos, and K. Petraki, “Realistic neutron star constraints on bosonic asymmetric dark matter,” *Phys.*

- Rev. D* **87** no. 12, (2013) 123507, [arXiv:1301.6811 \[hep-ph\]](#).
- [102] J. Bramante, K. Fukushima, and J. Kumar, “Constraints on bosonic dark matter from observation of old neutron stars,” *Phys. Rev. D* **87** no. 5, (2013) 055012, [arXiv:1301.0036 \[hep-ph\]](#).
- [103] J. Bramante, K. Fukushima, J. Kumar, and E. Stopnitzky, “Bounds on self-interacting fermion dark matter from observations of old neutron stars,” *Phys. Rev. D* **89** no. 1, (2014) 015010, [arXiv:1310.3509 \[hep-ph\]](#).
- [104] M. I. Gresham and K. M. Zurek, “Asymmetric Dark Stars and Neutron Star Stability,” *Phys. Rev. D* **99** no. 8, (2019) 083008, [arXiv:1809.08254 \[astro-ph.CO\]](#).
- [105] R. K. Leane, T. Linden, P. Mukhopadhyay, and N. Toro, “Celestial-Body Focused Dark Matter Annihilation Throughout the Galaxy,” *Phys. Rev. D* **103** no. 7, (2021) 075030, [arXiv:2101.12213 \[astro-ph.HE\]](#).
- [106] FCC Collaboration, A. Abada *et al.*, “FCC Physics Opportunities: Future Circular Collider Conceptual Design Report Volume 1,” *Eur. Phys. J. C* **79** no. 6, (2019) 474.
- [107] FCC Collaboration, A. Abada *et al.*, “FCC-ee: The Lepton Collider: Future Circular Collider Conceptual Design Report Volume 2,” *Eur. Phys. J. ST* **228** no. 2, (2019) 261–623.
- [108] M. Cobal, C. De Dominicis, M. Fabbrihesi, E. Gabrielli, J. Magro, B. Mele, and G. Panizzo, “Z-boson decays into an invisible dark photon at the LHC, HL-LHC and future lepton colliders,” *Phys. Rev. D* **102** no. 3, (2020) 035027, [arXiv:2006.15945 \[hep-ph\]](#).
- [109] T. Han, Z. Liu, L.-T. Wang, and X. Wang, “WIMPs at High Energy Muon Colliders,” *Phys. Rev. D* **103** no. 7, (2021) 075004, [arXiv:2009.11287 \[hep-ph\]](#).
- [110] R. Mahbubani, P. Schwaller, and J. Zurita, “Closing the window for compressed Dark Sectors with disappearing charged tracks,” *JHEP* **06** (2017) 119, [arXiv:1703.05327 \[hep-ph\]](#). [Erratum: *JHEP* 10, 061 (2017)].
- [111] H. Fukuda, N. Nagata, H. Otono, and S. Shirai, “Higgsino Dark Matter or Not: Role of Disappearing Track Searches at the LHC and Future Colliders,” *Phys. Lett. B* **781** (2018) 306–311, [arXiv:1703.09675 \[hep-ph\]](#).
- [112] M. Saito, R. Sawada, K. Terashi, and S. Asai, “Discovery reach for wino and higgsino dark matter with a disappearing track signature at a 100 TeV pp collider,” *Eur. Phys. J. C* **79** no. 6, (2019) 469, [arXiv:1901.02987 \[hep-ph\]](#).
- [113] R. Capdevilla, F. Meloni, R. Simoniello, and J. Zurita, “Hunting wino and higgsino dark matter at the muon collider with disappearing tracks,” *JHEP* **06** (2021) 133, [arXiv:2102.11292 \[hep-ph\]](#).
- [114] R. Capdevilla, F. Meloni, and J. Zurita, “Discovering Electroweak Interacting Dark Matter at Muon Colliders using Soft Tracks,” [arXiv:2405.08858 \[hep-ph\]](#).
- [115] T. Cohen, M. Lisanti, H. K. Lou, and S. Mishra-Sharma, “LHC Searches for Dark Sector Showers,” *JHEP* **11** (2017) 196, [arXiv:1707.05326 \[hep-ph\]](#).
- [116] K. R. Dienes, D. Kim, T. T. Leininger, and B. Thomas, “Sequential displaced vertices: Novel collider signature for long-lived particles,” *Phys. Rev. D* **106** no. 9, (2022) 095012, [arXiv:2108.02204 \[hep-ph\]](#).
- [117] G. D. Kribs and E. T. Neil, “Review of strongly-coupled composite dark matter models and lattice simulations,” *Int. J. Mod. Phys. A* **31** no. 22, (2016) 1643004, [arXiv:1604.04627 \[hep-ph\]](#).
- [118] L. Lee, C. Ohm, A. Soffer, and T.-T. Yu, “Collider Searches for Long-Lived Particles Beyond the Standard Model,” *Prog. Part. Nucl. Phys.* **106** (2019) 210–255, [arXiv:1810.12602 \[hep-ph\]](#). [Erratum: *Prog.Part.Nucl.Phys.* 122, 103912 (2022)].
- [119] J. Alimena *et al.*, “Searching for long-lived particles beyond the Standard Model at the Large Hadron Collider,” *J. Phys. G* **47** no. 9, (2020) 090501, [arXiv:1903.04497 \[hep-ex\]](#).
- [120] H. Chen, I. Moulton, X. Zhang, and H. X. Zhu, “Rethinking jets with energy correlators: Tracks, resummation, and analytic continuation,” *Phys. Rev. D* **102** (Sep, 2020) 054012. <https://link.aps.org/doi/10.1103/PhysRevD.102.054012>.
- [121] K. Lee and I. Moulton, “Energy Correlators Taking Charge,” [arXiv:2308.00746 \[hep-ph\]](#).
- [122] CMS Collaboration, A. Hayrapetyan *et al.*, “Measurement of energy correlators inside jets and determination of the strong coupling $\alpha_S(m_Z)$,” *Phys. Rev. Lett.* **133** (Aug, 2024) 071903. <https://link.aps.org/doi/10.1103/PhysRevLett.133.071903>.
- [123] M. Baumgart, T. Cohen, I. Moulton, N. L. Rodd, T. R. Slatyer, M. P. Solon, I. W. Stewart, and V. Vaidya, “Resummed Photon Spectra for WIMP Annihilation,” *JHEP* **03** (2018) 117, [arXiv:1712.07656 \[hep-ph\]](#).
- [124] L. Rinchuso, N. L. Rodd, I. Moulton, E. Moulin, M. Baumgart, T. Cohen, T. R. Slatyer, I. W. Stewart, and V. Vaidya, “Hunting for Heavy Winos in the Galactic Center,” *Phys. Rev. D* **98** no. 12, (2018) 123014, [arXiv:1808.04388 \[astro-ph.HE\]](#).
- [125] M. Baumgart, T. Cohen, E. Moulin, I. Moulton, L. Rinchuso, N. L. Rodd, T. R. Slatyer, I. W. Stewart, and V. Vaidya, “Precision Photon Spectra for Wino Annihilation,” *JHEP* **01** (2019) 036, [arXiv:1808.08956 \[hep-ph\]](#).
- [126] M. Baumgart, N. L. Rodd, T. R. Slatyer, and V. Vaidya, “The quintuplet annihilation spectrum,” *JHEP* **01** (2024) 158, [arXiv:2309.11562 \[hep-ph\]](#).
- [127] D. Djukanovic, J. Gegelia, and U.-G. Meißner, “Triviality of quantum electrodynamics revisited,” *Commun. Theor. Phys.* **69** no. 3, (2018) 263, [arXiv:1706.10039 \[hep-th\]](#).
- [128] D. S. M. Alves, J. Galloway, J. T. Ruderman, and J. R. Walsh, “Running Electroweak Couplings as a Probe of New Physics,” *JHEP* **02** (2015) 007, [arXiv:1410.6810 \[hep-ph\]](#).
- [129] X. Bekaert and N. Boulanger, “Tensor gauge fields in arbitrary representations of $GL(D,R)$. II. Quadratic actions,” *Commun. Math. Phys.* **271** (2007) 723–773, [arXiv:hep-th/0606198](#).
- [130] V. Berestetskii, E. Lifshitz, and L. Pitaevskii, *Quantum Electrodynamics: Volume 4*. Course of theoretical physics. Elsevier Science, 1982. <https://books.google.com/books?id=URL5NKX8vbAC>.
- [131] J. F. Donoghue, E. Golowich, and B. R. Holstein, *Dynamics of the standard model*, vol. 2. CUP, 2014.

- [132] D. J. Griffiths and D. F. Schroeter, *Introduction to Quantum Mechanics*. Cambridge University Press, 3 ed., 2018.
- [133] M. D. Schwartz, *Quantum Field Theory and the Standard Model*. Cambridge University Press, 3, 2014.
- [134] M. E. Peskin and D. V. Schroeder, *An Introduction to quantum field theory*. Addison-Wesley, Reading, USA, 1995.
- [135] G. M. Prosperini, M. Raciti, and C. Simolo, “On the running coupling constant in QCD,” *Prog. Part. Nucl. Phys.* **58** (2007) 387–438, [arXiv:hep-ph/0607209](#).
- [136] R. Corless, G. Gonnet, D. Hare, D. Jeffrey, and D. Knuth, “On the lambert W function,” *Advances in Computational Mathematics* **5** (01, 1996) 329–359.